Large-Scale Air-Sea Interactions in the Western Tropical Pacific

西部熱帯太平洋の大規模な大気・海洋相互作用の研究

升本　順夫

Large-Scale Air-Sea Interactions in the Western Tropical Pacific

西部熱帯太平洋の大規模な大気・海洋相互作用の研究

by

Yukio Masumoto

升本　順夫

Abstract

Large-scale air-sea interactions in the western tropical Pacific are investigated by use of simple atmosphere-ocean coupled models and a fine-resolution oceanic general circulation model (OGCM). First of all, the generation and evolution of an air-sea coupled disturbance relevant to the El Niño/Southern Oscillation (ENSO) phenomenon is investigated using a simple coupled aqua-planet model composed of Gill's moist atmosphere model and Anderson-McCreary's ocean model. A coherent air-sea coupled disturbance with zonal wavenumber one emerges from different initial disturbances either in the atmosphere or the ocean and propagates eastward. In the case of an initial westerly wind burst, oceanic Kelvin waves generated by the winds cause weak but long-lasting ocean temperature anomalies which trigger the air-sea coupled disturbance. When the initial disturbance is in the oceanic mixed-layer temperature, the coupled disturbance is excited more easily because the relaxation time is long in the ocean compared to the atmosphere. This is consistent with the result that the coupled disturbance collapses when the disturbance is forced to vanish on the oceanic side rather than on the atmospheric side.

In order to clarify the effect of a land process, the origin of an air-sea coupled disturbance in the Anderson-McCreary (1985a) type model is investigated in detail. The land process is included as an external heating west of the model Pacific. It is demonstrated that nonlinearities in the Anderson-McCreary type models dramatically change the state predicted by the linear theory. The repetitious generation of the coupled disturbance has nothing to do with the linear U1 mode of Hirst (1988) as well as off-equatorial Rossby waves. It is perfectly determined by the amplitude of the external heating. The mass budget analysis demonstrates that the change of zonal wind direction in the western Pacific, which is due to the relative importance between the external land heating and the heating associated with the previous coupled disturbance, modulates the oceanic heat content relevant to the origin of the following coupled disturbance. This mechanism gives an oscillation between two stable equilibria (La Niña and El Niño), which is very different from those described in Battisti (1988), Schopf and Suarez (1988), and Zebiak and Cane (1987).

Lastly, a fine-resolution OGCM based on the GFDL model is used to investigate the seasonal variability of the oceanic conditions in the western tropical Pacific. In particular, the seasonal evolution of the Mindanao Dome off the Philippine coast is examined. It is found that the model's Mindanao Dome evolves in late fall due to local upwelling when a positive wind-stress curl associated with the northeast Asian winter monsoon increases over the region. It expands eastward with a recirculation composed of the North Equatorial Current in the north, the Mindanao Current in the west, and the

North Equatorial Countercurrent in the south. After reaching a maximum in winter, it begins to decay in spring due to an intrusion of downwelling long Rossby waves excited in winter by the northeast trade winds farther eastward near 160°E, as well as a retreat of the local positive wind-stress curl. Further control runs demonstrate that the variation of the model's Mindanao Dome is almost totally determined by the change of the wind field in the western Pacific west of the date line.

The above numerical studies suggest that the Asian monsoon systems, i.e. the coupled ocean-atmosphere-land system, may strongly regulate the seasonal and interannual variabilities in the western tropical Pacific associated with short-term climate changes.

TABLE OF CONTENTS

Acknowledgements

I would like to express my sincere thanks to Dr. T. Yamagata, who stimulated my interest in this topic and contributed essentially to the progress of the work, and to Prof. A. Maeda and Dr. M. Sakurai, who gave me the opportunity to face with this field. I wish to thank Dr. K. Bryan, late M. Cox and Mr. R. Pacanowski for making the GFDL-OGCM available. Discussions with Drs. R. Lukas, D.X. Hu, and J. McCreary were of considerable benefit to me during the course of the work. Valuable comments on portions of this work were provided by Drs. D.S. Battisti, R. Lukas and M. Tsuchiya. My thanks also to the remainder of my thesis committee; Professors. Y. Nagata, A. Sumi, N. Suginohara and Dr. M. Kawabe.

I am indebted to the staff and students in Research Institute for Applied Mechanics/Kyushu University, at where most of this work has been done, for valuable discussions and providing a comfortable environment to do science over the years. I also gratefully acknowledge the very important moral and financial support by my family.

Finally, I would like to express my deepest gratitude, for showing the greatness of nature and providing fun of life, to the ocean.

Chapter 1 : Introduction

The western equatorial Pacific is characterized by its complexity of atmospheric and oceanic variabilities. From the perspective of a short-term climate change, various spatial and temporal scale phenomena, from atmospheric synoptic disturbances to decadal time-scale variations in both mediums, and their mutual interactions in the equatorial Pacific have been investigated for the last two decades (e.g., Madden and Julian, 1972; Keen, 1982; Barnet et al., 1989; Barnet, 1991). Among them, the El Niño/Southern Oscillation (ENSO) phenomenon has become the subject of world attention because of its extremely anomalous condition in the equatorial Pacific and its impact on the global climate. The ENSO sheds a bright light on an atmosphere-ocean coupled system in the equatorial Pacific.

Philander et al.(1984) demonstrated, by use of a simplified coupled atmosphere-ocean numerical model, that an unstable air-sea coupled disturbance appears in the system and that a positive air-sea feedback mechanism plays an important role during its evolution stage. To detect the unstable modes inherent in various coupled systems and clarify their underlying mechanism, there are many attempts to apply the linear stability analyses to the systems (e.g. Yamagata , 1985; Gill, 1985; Hirst, 1986, 1988; Hirst and Lau, 1989; Wakata and Sarachik, 1990). These studies showed that there are several types of atmosphere-ocean coupled unstable modes. Yamagata (1985) indicated that the oceanic equatorial Kelvin waves propagating to the east become unstable in a system in which the oceanic mixed-layer temperature anomaly is directly proportional to the mixed-layer depth anomaly. Rennick (1983) and Gill (1985), however, demonstrated that the westward propagating oceanic Rossby waves are unstable when the mixed-layer temperature anomaly is determined mainly by advection of a prescribed background temperature gradient. Although the degree of stability of each mode depends on the dynamics and thermodynamics of the coupled systems, those results confirmed the importance of the air-sea positive feedback mechanism to the coupled unstable modes.

After Philander et al.(1984)'s work, several air-sea coupled models with various levels of complexity have been constructed to investigate the coupled system in detail and simulate and/or predict short-term climate variabilities such as the ENSO phenomena (see McCreary and Anderson, 1991 for the review article). The hierarchy ranges from conceptual models, which are composed of only few variables and a set of drastically reduced equations (e.g. Lau, 1981; Vallis, 1988; Graham and White, 1988), to coupled general circulation models (GCMs) (e.g. Philander et al., 1989; Gordon, 1989; Nagai et al., 1992; see Neelin et al., 1991 for the review article). In particular, the models classified as simple or intermediate complexity, which consists of reduced-gravity ocean and atmosphere, have been contributing to a deeper understanding of the mechanism involved in the coupled systems (e.g. Anderson and McCreary, 1985a; Zebiak and Cane, 1987; Xie et al., 1989; Budin and Davey, 1989). This is because those models utilize more realistic dynamics and thermodynamics compared with the conceptual models and can reproduce realistic interannual variabilities. Furthermore, it is easy to determine the underlying mechanism at work in the models compared to the highly sophisticated coupled GCMs.

Anderson and McCreary (1985a), for example, developed an air-sea coupled model that consists of a reduced-gravity ocean and atmosphere with realistic ocean thermodynamics. It simulated successfully an eastward propagating ENSO-like disturbance with a period of about 4.5 years. Zebiak and Cane (1987), however, showed oscillatory solutions with stationary instabilities in the central and eastern Pacific at an interannual time-scale similar to ENSO, utilizing the reduced-gravity oceanic and atmospheric models, which include the surface mixed-layer in the ocean and the moist process in the atmosphere. Schopf and Suarez (1988) also indicated an irregular oscillation at ENSO time-scales using a 2 1/2-layer reduced gravity ocean model and a 2-layer atmospheric GCM.

Despite those successes in reproducing ENSO-like oscillations, many processes in the ENSO phenomena such as the onset and termination of the warm events are still

controversial issues. Schopf and Suarez (1988) demonstrated that the oscillated solutions in their model were attributed to the generation of oceanic Rossby waves in the equatorial wave guide associated with the previous coupled disturbance and its reflection at the western boundary; the mechanism is referred to as "the delayed action oscillator". Battisti (1988) analyzed in detail the results from their air-sea coupled model similar to the model of Zebiak and Cane (1987) and reached the same conclusion. The western boundaries of the Pacific Ocean in these models are merely a reflector for the equatorial waves. The atmosphere plays only a passive role in this mechanism in the sense that the seeds of the coupled disturbance are generated within the ocean.

On the other hand, Keen (1982), Nitta and Motoki (1987), and Nitta (1989) suggested that the warm event of the ENSO phenomena may be triggered by westerly wind bursts in the equatorial western Pacific and subsequent eastward redistribution of positive sea surface temperature (SST) anomaly in the western and central tropical Pacific. The atmosphere plays an active role in generating the coupled disturbance during this time. It is important, therefore, to clarify the most favorable condition for the coupled disturbance to occur and the relation between the atmospheric intraseasonal variability and the air-sea coupled interannual disturbance under a simple situation, e.g., with a cyclic ocean and atmosphere. Chapter 2 investigates in detail the generation and evolution mechanism of the air-sea coupled disturbance in a simple aqua-planet model with different initial conditions to address the above issues.

In contrast to the delayed action oscillator mechanism, it has been suggested that the externally imposed land heating west of the model Pacific Ocean (Q_L) is crucial to generate the recurrent eastward propagating air-sea coupled disturbance in models similar to the one used by Anderson and McCreary (1985a) (hereafter referred to as AM type models) (Anderson and McCreary, 1985b; Yamagata and Masumoto, 1989; Budin and Davey, 1989). With $Q_L = 0$ or with a sufficiently large Q_L, the system adjusts to an equilibrium state with a warm mixed-layer temperature in the eastern Pacific or a cool mixed-layer temperature there, respectively. Only with moderate heating can the model

produce an oscillatory state. However, the mechanisms for evolution of the coupled disturbances in the western Pacific in the AM type models have not been investigated. It should be clarified whether the delayed action oscillator mechanism plays a crucial role in the AM type models or the recurrence of the disturbances is governed by a different mechanism. Thus, Chapter 3 deals with the underlying mechanism for the generation of the coupled disturbance in the AM type models in detail, and shows that the external land heating is important in recurrence of the model ENSO.

Not only the results from the numerical models but also analyses of the observed variables offer significant information to improve our knowledge regarding the air-sea coupled system. The composite picture of ENSO phenomena shows that the oceanic heat content (OHC) and the sea level height in the western tropical Pacific increase in association with the anomalously strong easterlies over the region prior to the El Niño events (cf. Wyrtki, 1985; Cane, 1986). In particular, White et al. (1987) analyzed the OHC field derived from expendable bathythermograph temperature (XBT) profiles and indicated that a positive OHC anomaly appears off the Philippine coast in late fall prior to the warm ENSO. Meehl (1987) showed that the SST variability in the equatorial western Pacific is an important constituent of the dynamically coupled ocean-atmosphere system in the Indian-Pacific region for annual and interannual time-scales. Recently, Yasunari (1991) demonstrated a high positive correlation between the strong Indian summer monsoon and the positive OHC anomaly in the western tropical Pacific in the following winter. These analyses suggest that the precondition for the El Niño is strongly affected by the seasonal variability of the ocean-atmosphere-land coupled system in the western Pacific, e.g., the Asian monsoon systems.

To understand the anomalous conditions in the western tropical Pacific and to have a clearer perception of the phase relation between the ENSO phenomena and the seasonal cycle in the equatorial Pacific, the mechanism that determines the basic fields in the region must be elucidated as well. However, our knowledge of the mean field and especially the seasonal variability in the western tropical Pacific is very limited, since

available observed data is sparse in time and space and there has been a lack of numerical studies focusing on the seasonal cycle in this area. Therefore, in Chapter 4, the seasonal variations of the oceanic basic field for the coupled disturbance are studied using a fine-resolution oceanic GCM. In particular, the seasonal evolution of the cold region off the Philippine coast (the Mindanao Dome) is studied in terms of the response of the western tropical Pacific to the Asian monsoonal wind system.

Chapters 2 to 4 of this dissertation consist of separate works which have been published. Chapter 2 has been printed in "Meteorology and Atmospheric Physics" in 1990 under the title "The birth and evolution of an eastward propagating air-sea coupled disturbance in an aqua-planet". Chapter 3 was published in "Journal of the Meteorological Society of Japan" in 1991 with the title "On the origin of a model ENSO in the western Pacific". Chapter 4 has been published in "Journal of Physical Oceanography" in 1991; the title is "Response of the western tropical Pacific to the Asian winter monsoon: the generation of the Mindanao Dome".

Chapter 2 : Favorable Condition for an Air-Sea Coupled Disturbance

2.1 Introduction to Chapter 2

As is stated in Chapter 1, nowadays, no one doubts that an air-sea positive feedback plays a key role during the evolution of ENSO events (see Philander et al., 1984 ; Yamagata, 1985 ; Hirst, 1986 ; 1988). Several air-sea coupled models of various levels of complexity have recently been developed along the above line and used to simulate the ENSO phenomena. In particular, some models reproduced successfully ENSO-like oscillatory behaviors (e.g. Anderson and McCreary, 1985a ; Zebiak and Cane, 1987 ; Schopf and Suarez, 1988 ; Philander et al., 1989). The consequence is that our understanding of the *model ENSO* has been extremely advanced in recent years (Battisti, 1988 ; Yamagata and Masumoto, 1989 ; Davey and Budin, 1989).

However, several key stages of the *actual ENSO* are still not well understood. Those are, for example, onset and termination phases of a warm event. In particular, it is still a matter of controversy whether atmospheric intraseasonal disturbances may trigger such a long-lasting warm coupled disturbance, i.e. the interannual ENSO mode (Wang and Murakami, 1988). Schopf and Suarez (1988) demonstrated that the birth of a warm coupled disturbance in their *model ENSO* may be attributed to off-equatorial oceanic Rossby waves excited during a cold event which follows the previous warm event. The oceanic Rossby waves are transformed into warm Kelvin waves after reflection at the western boundary of the model Pacific, and then give rise to the air-sea coupled disturbance propagating eastward. Battisti (1988) has also studied in detail his coupled model results almost identical to those of Zebiak and Cane (1987) and reached the same conclusion. Keen (1982), Nitta and Motoki (1987) and Nitta (1989), however, suggested that the *actual ENSO* events may be triggered in the western Pacific by atmospheric westerly bursts associated with cross-equatorial cyclones. Recently, Yamagata and Masumoto (1989) pursued the same issue and suggested that both

atmospheric westerly bursts and warm oceanic heat content (OHC) anomaly in the western tropical Pacific are necessary conditions for the warm ENSO event.

In reality atmospheric and/or oceanic disturbances may possibly generate the air-sea coupled disturbance. A key question we raise here is what is more favorable and what is an underlying mechanism to generate or to kill the coupled disturbance. This basic problem needs to be well understood in the perspective of ENSO turnabouts which were skipped by Bjerknes (1966), but are of present concern. In order to focus attention on the problem, we adopt a simple aqua-planet ocean-atmosphere coupled model in this chapter. A more detailed model description is given in Section 2.2. Section 2.3 describes some numerical results relevant to birth and demise of the air-sea coupled disturbance. Conclusions and discussion for Chapter 2 is given in Section 2.4.

2.2 Description of a Coupled Aqua-planet Model

2.2.1 Model Atmosphere

The model atmosphere is the spherical version of Gill (1982)'s moist model (Yamagata, 1987 ; Davey and Gill, 1987) and covers the area from 50°S to 50°N with the $4^\circ \times 2^\circ$ grid resolution. The rudiments on an f-plane are given by Gill (1982). Here we begin with the equations for a primitive, one-mode atmosphere on a sphere. The linearized momentum equations have the form

$$\frac{\partial U}{\partial t} - fV = -\frac{1}{\rho_a a \cos\phi}\frac{\partial p}{\partial \lambda} - \varepsilon U, \tag{1a}$$

$$\frac{\partial V}{\partial t} + fU = -\frac{1}{\rho_a a}\frac{\partial p}{\partial \phi} - \varepsilon V, \tag{1b}$$

where (U,V) denote the horizontal velocities at the lower troposphere, p the pressure perturbation, ρ_a air density, f the Coriolis parameter, and a is the radius of the earth. Variables (λ,ϕ) represent longitude and latitude, respectively, and the constant ε is the

coefficient for Rayleigh damping (0.2 per day). The continuity equation applied to the lower troposphere is written in the form

$$\frac{\partial U}{a \cos\phi \, \partial\lambda} + \frac{\partial V}{a \, \partial\phi} + \frac{W}{H_o} = 0 , \tag{2}$$

where H_o is the depth of lower troposphere and W is the vertical velocity at the middle level of the troposphere. Assuming the hydrostatic balance leads to the equation which relates p with the potential temperature perturbation θ. This has the form

$$p = - \rho_a g H_o \frac{\theta}{\theta_o} , \tag{3}$$

where g is the acceleration due to gravity and θ_o is the typical potential temperature. The potential temperature perturbation at the middle level of troposphere is governed by

$$\frac{\partial \theta}{\partial t} + \frac{\theta_o N^2}{g} W = Q - \gamma_a \theta, \tag{4}$$

where N is the buoyancy frequency, γ_a is the coefficient of Newtonian cooling (0.2 per day) and Q is the heating rate. This Q is related to the precipitation rate P in the following form

$$Q = \frac{\rho_w L_c P}{\rho_a H_o C_p} , \tag{5}$$

where ρ_w is the water density, L_c is the latent heat of condensation, and C_p is the specific heat of air at constant pressure. The precipitation rate P is predicted by the linearized equation which governs the moisture per unit area:

$$E - \overline{q}\left(\frac{\partial U}{a\cos\phi\,\partial\lambda} + \frac{\partial V}{a\,\partial\phi}\right) = P \qquad \text{for } q = \overline{q} \text{ and } P > 0, \tag{6a}$$

and

$$\frac{\partial q}{\partial t} + \overline{q}\left(\frac{\partial U}{a\cos\phi\,\partial\lambda} + \frac{\partial V}{a\,\partial\phi}\right) = E \qquad \text{for } q < \overline{q} \text{ or } q = \overline{q} \text{ and } P < 0, \tag{6b}$$

where $\overline{q}$ is the amount of moisture in a column per unit area expressed by a depth of liquid water, for which the atmosphere is just saturated. We assume that $\overline{q}$ is always given by the saturated value at 28°C (7.0cm). The perturbation evaporation E is given by

$$E = -\delta\,(q - q_s(T_s)), \tag{7}$$

where δ is a measure of the relaxation process (0.14 per day) for the moisture content and q_s is the saturated moisture at the sea surface temperature T_s, which is calculated in the ocean model. Linearizing the Clapeyron-Clausius relation around the saturated moisture q at 28°C, we obtain

$$q_s(T_s) = \overline{q}\,(1 + 0.058\,(T_s - 28)). \tag{8}$$

Now it is convenient to introduce a new quantity H defined by

$$H \equiv \frac{H_o\theta}{\theta_o} \quad \left(= -\frac{p}{\rho_a g}\right). \tag{9}$$

Then the potential temperature equation (4) is replaced by

$$\frac{\partial H}{\partial t} - (H_e - H_m)\left(\frac{\partial U}{a\cos\phi\,\partial\lambda} + \frac{\partial V}{a\,\partial\phi}\right) = \Delta E - \gamma_a H$$

$$\text{for } q = \overline{q} \text{ and } P > 0, \qquad (10a)$$

and

$$\frac{\partial H}{\partial t} - H_e\left(\frac{\partial U}{a\cos\phi\,\partial\lambda} + \frac{\partial V}{a\,\partial\phi}\right) = -\gamma_a H$$

$$\text{for } q < \overline{q} \text{ or } q = \overline{q} \text{ and } P < 0, \qquad (10b)$$

where

$$\Delta = \frac{\rho_w L_c}{\rho_a \theta_o C_p}. \qquad (11)$$

The equivalent depth H_e ($= N^2 H_o^2/g$) and the negative contribution due to moist processes H_m ($= \rho_w L_c \overline{q}/(\rho_a \theta_o C_p)$) are used for simplicity. We assume H_e = 450m and H_m = 395m. These values ensure that the present moist process is stable, because the effective equivalent depth (H_e - H_m) is kept positive. In other words, the warming due to the latent heat release is smaller than the cooling due to vertical advection of sensible heat.

2.2.2 Model Ocean

The model ocean is the spherical version of the Anderson-McCreary model and covers the whole globe from 50°S to 50°N with the 2° × 1° grid resolution. The reason we adopt the model is that it is the simplest model which includes the ocean thermodynamics explicitly. The details are described in the original paper (Anderson and McCreary, 1985a). Here we only refer to the equations. Those are

$$\frac{\partial(\mathbf{hu})}{\partial t} + \mathbf{u}.\nabla(\mathbf{hu}) + \mathbf{hu}\,\nabla.\mathbf{u} - f\mathbf{k}\times(\mathbf{hu}) = -\nabla\left(\frac{1}{2}\alpha g T h^2\right) + \nu_h \nabla^2(\mathbf{hu}) + \tau, \qquad (12a)$$

$$\frac{\partial h}{\partial t} + \nabla . (h\mathbf{u}) = \frac{2\delta_o}{h^2 T} - w + \gamma_o (\frac{T - T^*}{T}), \tag{12b}$$

$$\frac{\partial T}{\partial t} + \mathbf{u} . \nabla T = \frac{2}{h} (-\gamma_o (T - T^*) - \frac{\delta_o}{h^2}) + \nu_h \nabla^2 T, \tag{12c}$$

where T is the mixed-layer temperature minus that of the deep layer (19.5°C in the present model), h the thickness of the upper layer, **u** the horizontal current velocity vector, τ the wind stress proportional to the wind (U,V) as in Anderson and McCreary (1985a), and f, g, t, **k** are the Coriolis parameter, the acceleration due to gravity, the time, and the vertical unit vector, respectively. The values of lateral eddy viscosity ν_h, thermal expansion coefficient α, upwelling velocity from the deep layer w, entrainment coefficient δ_o, and thermal relaxation coefficient γ_o are 5×10^7 cm^2/s, 3×10^{-4} $°C^{-1}$, 4×10^{-5} cm/s, 4×10^4 $cm^3°C/s$, and 3×10^{-4} cm/s, respectively. The sea surface temperature T_s, which appears in Eq. (8) for the atmosphere, is given by

$$T_s = T + 19.5. \tag{13}$$

The reference temperature T^* exactly follows the expression of Anderson and McCreary (1985a) such as

$$T^* = 4 + (11.33 - 4) (1 + \cos 2\pi y/y_N) /2, \tag{14}$$

where $y_N = 90°$ in the present model. The steady solution without motion for the above set of thermal parameters has $\overline{T}$ = 10°C and $\overline{h}$ = 100m at the equator.

2.3 Birth and Evolution of an Air-Sea Coupled Disturbance

The air-sea coupled model described above was integrated by exchanging necessary information between the ocean and atmosphere once per half a model day. For the case of no initial disturbances (Figure 1), weak off-equatorial westward winds (of which magnitude is about 1 m/s) with double maxima near 25°N and 25°S are driven during initial adjustment processes by latent heating due to evaporation over the warm initial SST along the equator. These easterlies drive weak off-equatorward Ekman currents associated with upwelling of a tropical cold water as well as weak westward tropical currents (including a Yoshida jet) with a magnitude of less than 10 cm/s (see Yoshida, 1955 ; McCreary, 1981). The upwelling cools the sea surface temperature (SST) so that the coupled system finally ends up with no motion as discussed in Yamagata (1985). We note here that no growing coupled disturbance evolves in the present case.

2.3.1 A Case of an Initial Wind Anomaly

In this subsection we describe a response of the coupled system to an initial wind anomaly. We apply an external wind burst to the system for initial 5 days in the form of

$$U = A \exp \{ - (\frac{\lambda - 160^\circ}{30^\circ})^2 - (\frac{\phi}{10^\circ})^2 \}, \qquad (15)$$

where A is the amplitude of the disturbance, of which value is 10 m/s in the present simulation.

Figure 2 shows the longitude-time plots of (a) the zonal wind velocity and (b) the precipitation rate right on the equator for the case of a westerly burst. The initial wind convergence on the eastern end of the burst around 200° of the longitude leads to increased precipitation as shown in Yamagata (1987) for the uncoupled atmosphere. In the present case, however, the increased precipitation lasts for about 100 days and the

area propagates eastward with a phase speed of about 2 m/s. It turns out that the increased precipitation is caused by oceanic warm Kelvin waves excited by the burst.

Figure 3 shows the longitude-time sections of (a) the zonal current, (b) the mixed-layer temperature and (c) the depth of the mixed-layer right on the equator. It is clearly seen that there are two kinds of disturbances evolving in the system. Those are a quick oceanic disturbance during the first few hundred days with an atmospheric response as a slave and a slow ocean-atmosphere coupled disturbance with the zonal wavenumber 1 emerged after about Day 400. The westerly burst initially excites oceanic Kelvin waves which propagate eastward with a phase speed of about 2 m/s. This disturbance is associated with positive mixed-layer depth anomaly which goes around the globe. The positive temperature anomaly associated with this mixed-layer anomaly lasts for a few months and enhances precipitation on the atmospheric side. The quick response of this type eventually triggers the slowly evolving air-sea coupled disturbance which propagates eastward with a phase speed of about 0.4 m/s. The growth of the slow mode appears to be further accelerated by the returned fast mode going around the aqua-planet (Fig. 3a). This is not possible in the actual ocean with boundaries. However, as seen in Figs.2 and 3, the slow air-sea coupled mode evolves basically from the first encounter with the fast mode. Therefore it seems quite possible for the fast mode to generate the slow mode in reality. As is well-known for the actual warm ENSO mode, the present coupled disturbance is associated with positive mixed-layer depth and temperature anomalies and an enhanced precipitation along the equator.

The main difference between the quick response and the slow response is in the sign of the correlation between the winds and the currents (Yamagata, 1985). In the slow response the correlation is positive at least until Day 1000 so that the disturbance grows due to the positive feedback. In the quick response, however, the correlation is negative so that the disturbance fades out eventually. The initial westerly wind burst also excites oceanic Rossby waves which propagate westward with a phase speed of about 0.7 m/s as

seen in Fig. 3a. Note, however, that the Rossby waves are not associated with discernible mixed-layer depth and temperature anomalies on the equator (Matsuno, 1966).

Figure 4 shows horizontal structures of atmospheric pressure, winds and moisture for the well-developed air-sea coupled disturbance with the zonal wavenumber 1. The anomalous winds show the well-known Matsuno-Gill pattern composed of both stationary Rossby wave and Kelvin wave response (Matsuno, 1966 ; Gill, 1980). Figure 5 shows horizontal structures of oceanic mixed-layer depth, mixed-layer temperature, and current vectors for the coupled disturbance. It should be noted that the atmospheric low pressure, which induces wind convergence, is located just above the equatorial warm mixed-layer temperature anomaly associated with a deep mixed-layer. This structure of the air-sea coupled disturbance is consistent with the results of Philander et al.(1984), Yamagata (1985), Anderson and McCreary (1985a) and others.

It is also of interest to examine the case for an initial easterly wind burst. We apply the external wind burst to the system for initial 5 days in the same form with Eq.(15). The easterly burst excites oceanic Kelvin waves associated with a shallow mixed-layer (Figs. 6 and 7). This introduces a weak zonal variation into a uniform atmospheric heating through changes of the mixed-layer temperature. The variation in the atmospheric heating generates zonal wind convergence at 140°E after Day 50 with weak easterlies to the east and westerlies to the west (Fig.6a). This weak secondary westerlies related with the oceanic quick response lasts for a few months and finally triggers an air-sea coupled disturbance almost identical to the case for the westerly burst.

Here it is of interest to see how the atmospheric synoptic events such as the bursts prepare a condition favorable for the growth of the coupled disturbance in the present model. The secondary westerly related to the quick response on the oceanic side accumulates surface water near the equator and depresses the thermocline there. This depression reduces cold water entrainment and thus raises the mixed-layer temperature. The secondary easterly, on the other hand, decreases the mixed-layer temperature due to enhanced entrainment. Since the ocean mixed-layer temperature is not very sensitive to

the mixed-layer thermodynamics in the present model, the temperature variation due to the above effect is less than 0.1°C. Even if it is small, it lasts at least for a couple of months. This is because, in contrast to the initial atmospheric bursts which decay within 10 days, the secondary winds linger at least for a few months since they are driven by the oceanic Kelvin waves. The coherent air-sea coupled disturbance emerges eventually from this long-lasting oceanic decaying process. The present results suggest that in reality intraseasonal wind bursts may lead to the coherent air-sea coupled disturbance via a favorable oceanic condition.

2.3.2 A Case of an Initial SST Anomaly

In this subsection we discuss how an initial SST anomaly adapts in the coupled system. The SST anomaly we assume is in the form

$$T = B \exp \{ - (\frac{\lambda - 160^\circ}{30^\circ})^2 - (\frac{\phi}{10^\circ})^2 \}, \qquad (16)$$

where B is the amplitude of the disturbance and is assumed to be 0.5°C in the present simulation.

Figure 8 shows the longitude-time sections of (a) the zonal winds and (b) the precipitation rate on the equator. Figure 9 shows the longitude-time sections of (a) the zonal velocity, (b) the mixed-layer temperature and (c) the depth of the mixed-layer on the equator. The positive SST anomaly induces an excess evaporation and precipitation over the equator (Fig. 8b), and thus excites westerlies to the west and easterlies to the east (Fig.8a). The westerlies, in turn, support the SST anomaly on the equator due to the Ekman convergence so that the anomalous condition lasts for a few months (Fig. 9b). After 250 days, the anomalous area begins to move eastward with a phase speed of about 0.4 m/s. Notice that the air-sea coupled disturbance thus formed has the same structure as that discussed in the previous section. The time it takes to emerge is, however, only one half of that for the cases of the initial wind bursts; the air-sea coupled disturbance can

be excited more easily by the positive temperature anomaly in the ocean than by the wind anomaly in the atmosphere. This is because the effect of the ocean temperature anomaly on the coupled disturbance is more direct than that of the atmospheric winds.

2.3.3 Robustness of the Coupled Disturbance

It is also of interest to see how robust the air-sea coupled coherent disturbance is. In order to see this, we carried out two further experiments by taking special measures at the mature stage (Day 1000) of the case for the westerly burst (see Section 2.3.1).

In the first experiment, the atmospheric anomalies related to the coupled disturbance are forced to vanish at Day 1000. Figure 10 shows the longitude-time sections of (a) the zonal winds, (b) the rate of precipitation, (c) the zonal currents and (d) the mixed-layer temperature on the equator. The zonal winds associated with the coupled structure revive very rapidly in spite of the drastic steps and continue to grow as if no measures were taken. The oceanic component can produce again the atmospheric one since the relaxation time of the former is much longer than the latter one.

In the second experiment, the oceanic anomalies related to the coupled disturbance are forced to vanish at Day 1000. Figure 11 shows the longitude-time sections of (a) the zonal winds, (b) the rate of precipitation, (c) the zonal currents and (d) the mixed-layer temperature on the equator. Both atmospheric and oceanic components are seriously modified in the present case as compared with the first case. Immediately after disappearance of the oceanic anomalies, atmospheric ones decay quickly due to the Rayleigh damping. However, oceanic waves excited by the anomalous winds induce the mixed-layer depth and temperature anomalies which last for a few months, and thus gradually trigger the air-sea coupled disturbance. This revival process is quite similar to that for the westerly bursts discussed in Section 2.3.1.

2.4 Conclusions and Discussion for Chapter 2

In Chapter 2, we have investigated the evolution of an air-sea coupled disturbance propagating eastward in an aqua-planet. A robust coupled disturbance with the zonal wavenumber 1, which has properties quite similar to those of the disturbance leading to the warm ENSO event, emerges from different initial disturbances, either in the atmosphere or the ocean. In reality, the coupled disturbance with such a large zonal extent may be susceptible to existing meridional boundaries.

When the westerly bursts are applied to the coupled system, oceanic Kelvin waves generated by the winds cause weak but long-lasting ocean temperature fluctuations which trigger the air-sea coupled disturbance. It takes, however, rather long time in the present model for the atmospheric disturbance to excite the air-sea coherent structure of a finite amplitude. If we include the wind speed dependency on the evaporation, the atmospheric disturbance will last for longer time and the atmospheric triggering will be more effective. However, the time necessary to trigger the coupled mode appears to depend mainly on how sensitive the ocean temperature is to the oceanic quick response forced by the atmospheric disturbance.

When the initial disturbance consists of the oceanic mixed-layer temperature anomaly, the atmosphere responds directly in such a way that the Matsuno-Gill pattern forms above the warm SST. Since the oceanic relaxation time is long as compared to the atmospheric one, the perturbation remains for a long time and leads more easily to the coupled disturbance. In addition, the atmospheric winds generate currents and thermocline depression more favorable to the coupled disturbance. The present result suggests that, if the zonal extent of the perturbation is the same, the oceanic positive temperature anomaly can be a more direct trigger for the coupled disturbance.

The importance of the oceanic response is further consolidated from the results that the coupled disturbance may disappear when the disturbance is forced to vanish on the oceanic side. In contrast to this, the coupled disturbance suffers almost no influence when cutting the atmospheric component.

According to Wyrtki (1985), White et al. (1987) and Yasunari (1991), an anomalously warm region is formed in the western equatorial Pacific in winter before warm ENSO events. In addition to this, according to recent satellite observations the warm water with high SST quickly covered a wide region from the western Pacific to the central Pacific and thus formed a non-equilibrium state in the ocean-atmosphere coupled system. This quick eastward movement of the SST anomaly as a result of oceanic advection due to Kelvin waves has already been discussed by Gill (1983). After that, the warm air-sea coupled disturbance began to evolve (Nitta, 1986; Nitta and Motoki, 1987). These situations on the planet Earth seem to be consistent with those discussed in this chapter.

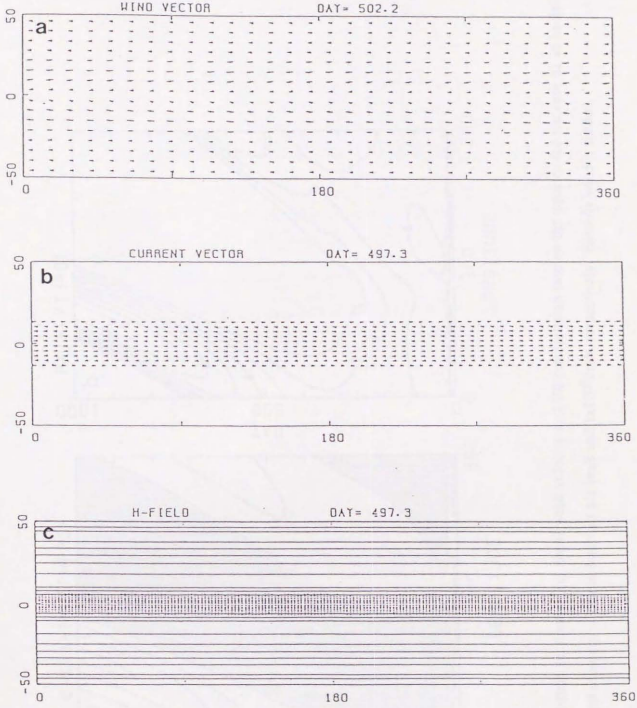

Fig.1. Horizontal structures of (a) wind vectors, (b) current vectors and (c) oceanic mixed-layer depth anomaly at Day 500 for the case of no initial disturbance. Contour interval is 10m. Negative anomalies are shaded.

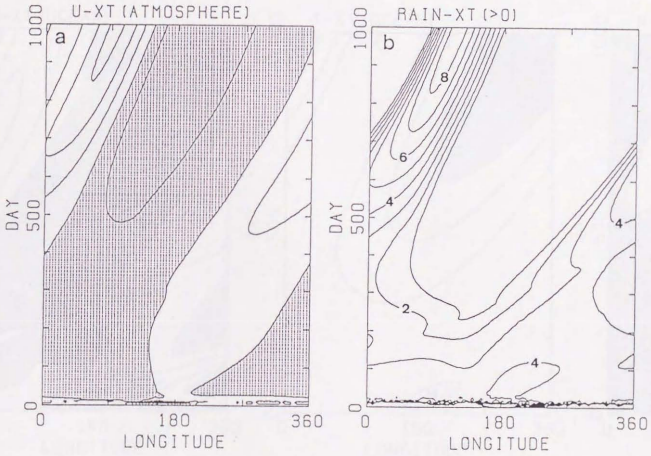

Fig.2. Longitude-time sections of (a) zonal wind velocity and (b) precipitation rate on the equator for the case of an initial westerly wind anomaly. Contour intervals are 1m/s and 1×10^{-6}cm/s, respectively. Easterly wind is shaded.

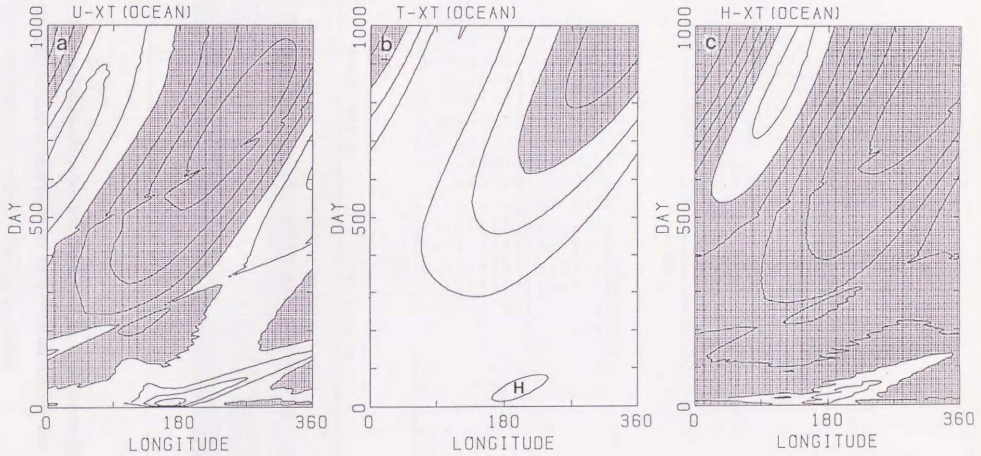

Fig.3. Longitude-time sections of (a) zonal current velocity, (b) mixed-layer temperature and (c) mixed-layer depth anomaly on the equator for the case of an initial westerly wind anomaly. Contour intervals are 10cm/s, 0.5°C and 10m, respectively. Westward flow, temperature less than 8.5°C and negative depth anomaly are shaded.

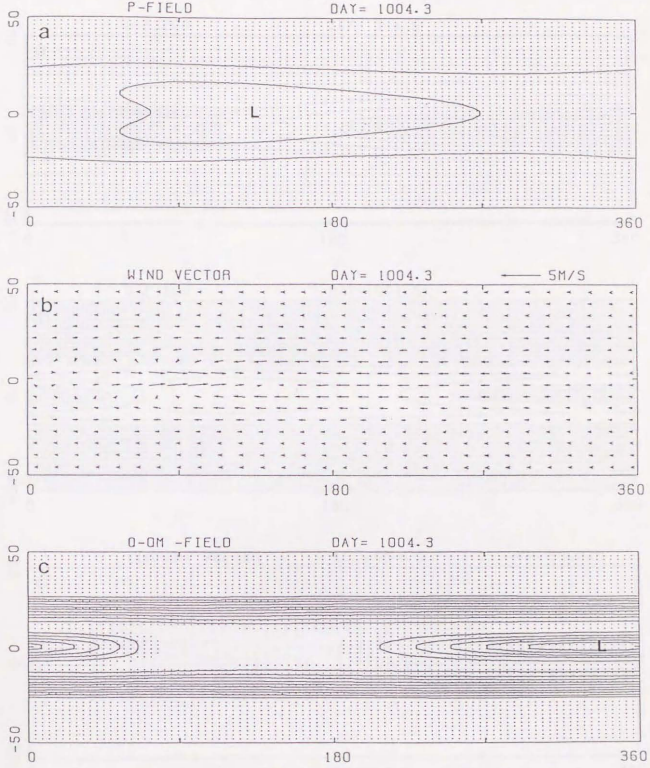

Fig.4. Horizontal structures of (a) atmospheric pressure, (b) winds and (c) moisture at Day 1004.3. Contour intervals for the pressure and the moisture field are 5×10^3cm and 0.1cm, respectively. Negative anomalies are shaded.

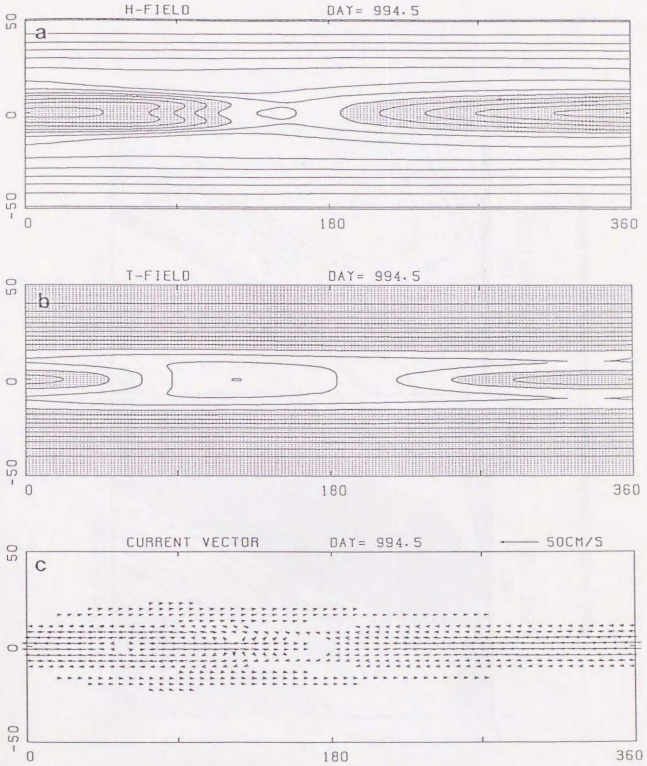

Fig.5. Horizontal structures of (a) oceanic mixed-layer depth, (b) mixed-layer temperature and (c) current vectors at Day 994.5. Contour intervals are 10m and 0.5°C. Negative anomaly of the mixed-layer depth and the temperature less than 8.5°C are shaded. Current velocity vectors less than 1cm/s are not shown.

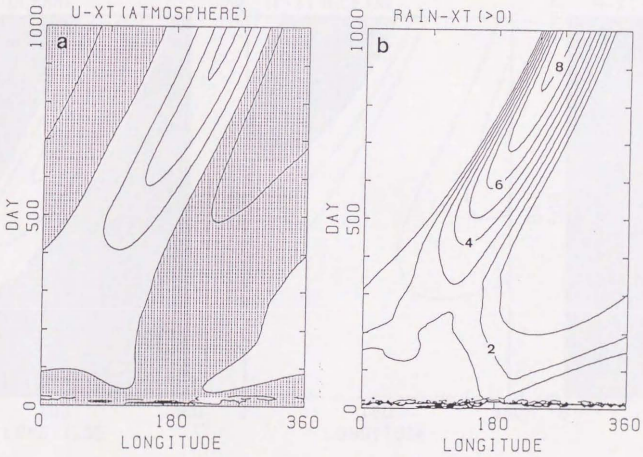

Fig.6. As in Fig.2 but for the case of an initial easterly wind anomaly.

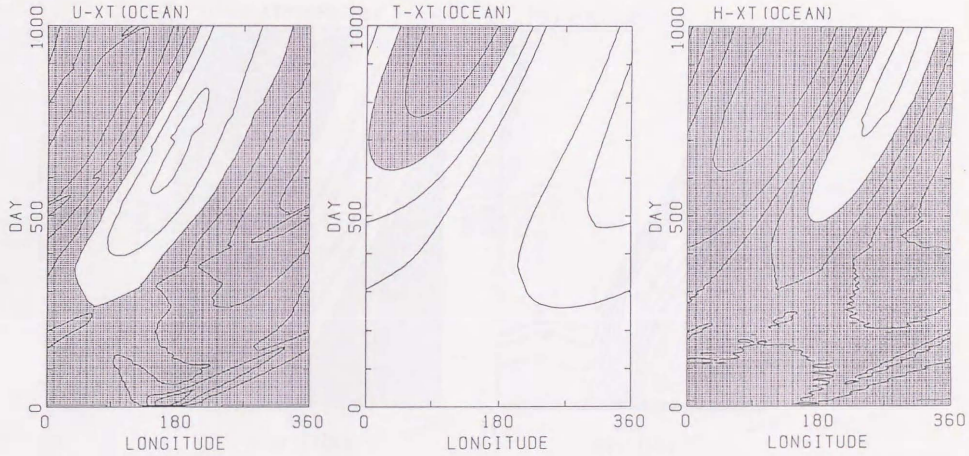

Fig.7. As in Fig.3 but for the case of an initial easterly wind anomaly.

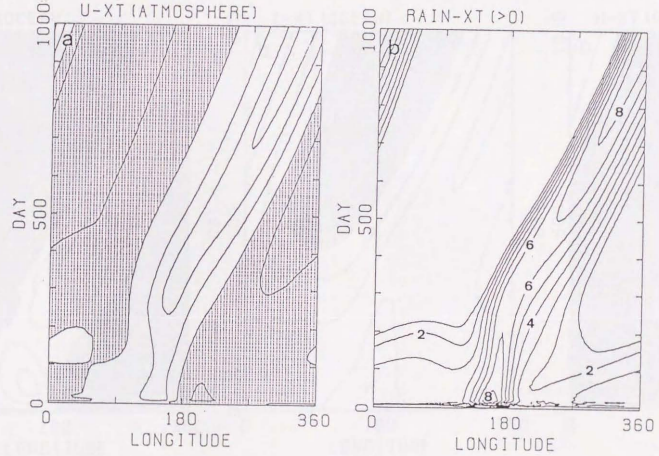

Fig.8. As in Fig.2 but for the case of an initial SST anomaly.

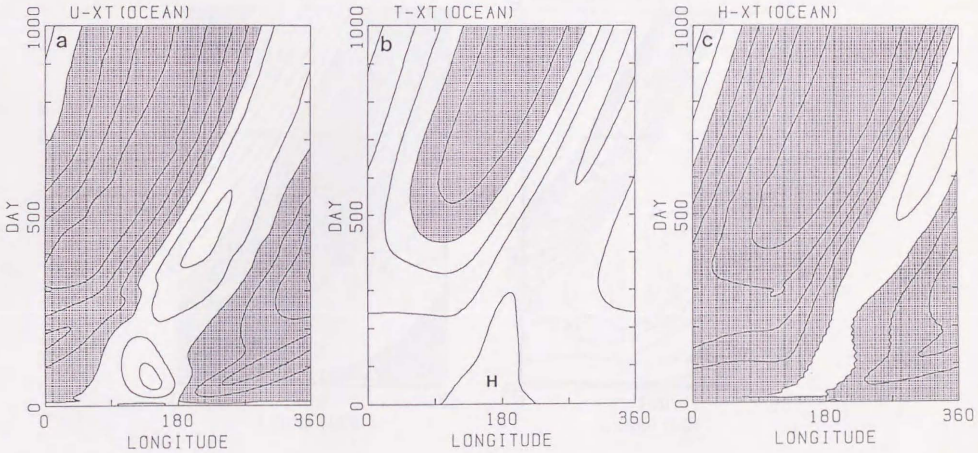

Fig.9. As in Fig.3 but for the case of an initial SST anomaly.

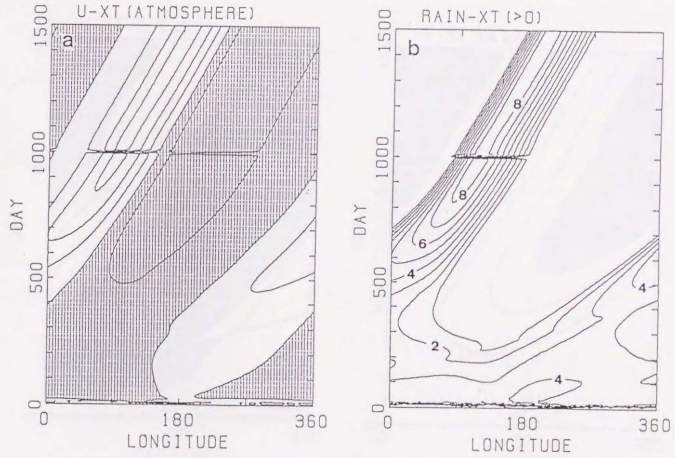

Fig.10. Longitude-time sections of (a) zonal wind velocity, (b) precipitation rate, (c) zonal current velocity and (d) mixed-layer temperature on the equator for the case that the atmospheric anomalies are forced to vanish at Day 1000. Contour intervals are 1m/s, 1×10^{-6}cm/s, 10cm/s and 0.5°C, respectively. Easterly wind, westward flow and mixed-layer temperature less than 8.5°C are shaded.

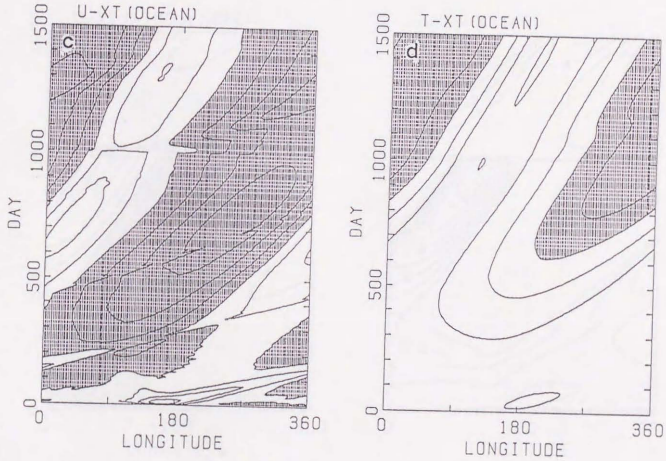

Fig.10. Continued.

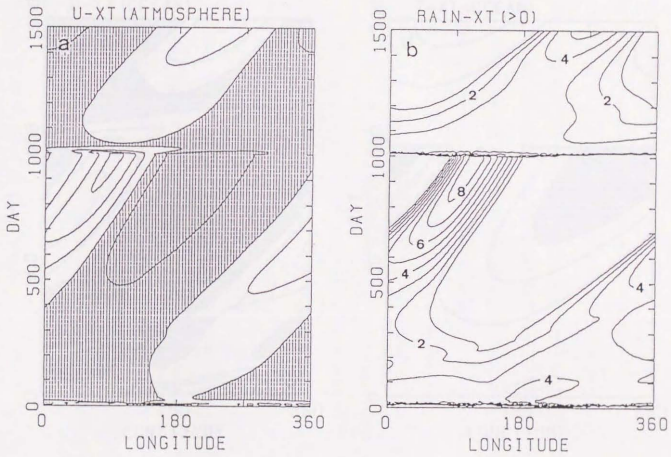

Fig.11. As in Fig.10 but for the case that the oceanic anomalies are vanished at Day 1000.

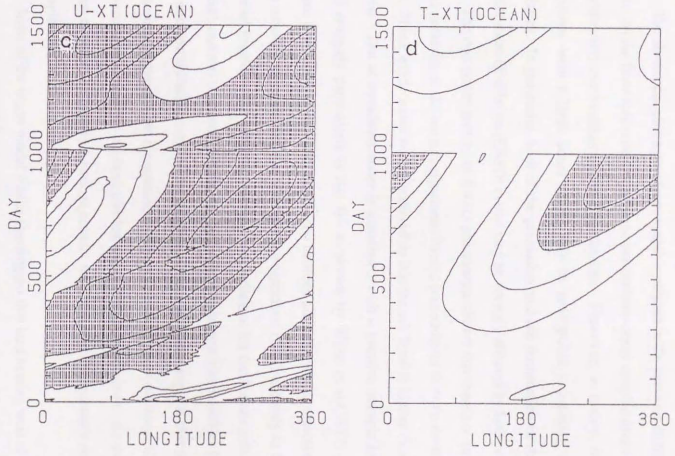

Fig.11. Continued.

Chapter 3 : Origin of a Model ENSO in the Western Pacific

3.1 Introduction to Chapter 3

The air-sea coupled aqua-planet model is utilized in the previous chapter in order to focus on the favorable conditions for the atmosphere-ocean coupled disturbances and the generation mechanisms of the disturbances. However, in reality, the coupled disturbance with a large zonal extent may be susceptible to existing meridional boundaries. In particular, both of the generation and the termination of the warm El Niño/Southern Oscillation (ENSO) events may be strongly affected by land processes.

The composite picture of ENSO phenomena shows that there are stronger than normal easterlies in the western equatorial Pacific preceding an El Niño event (cf. Cane, 1986). These winds move water westward so that the sea level is higher than normal in the west. The accumulated water is associated with a positive oceanic heat content (OHC) anomaly particularly in late fall as shown by White et al.(1987). Recently, Yasunari (1991) found very high correlation between all India rainfall associated with the Indian summer monsoon and the sea surface temperature (SST) anomaly in the western equatorial Pacific in the following winter. According to his further analysis, the active (inactive) summer monsoon is followed by increasing anomalous easterlies (westerlies) in the equatorial Pacific west of the dateline. These analyses suggest that the positive OHC anomaly appearing in the equatorial western Pacific prior to the warm ENSO event is a consequence of an air-sea-land process west of the Pacific ocean. As shown in the previous chapter, the above anomalous oceanic state is one of the necessary condition for the coupled disturbance to emerge.

Some of the recent model results also suggest that land heating west of the Pacific plays a key role during ENSO turnabouts (Anderson and McCreary, 1985a, hereafter referred to AM85; Yamagata and Masumoto, 1989 ; Budin and Davey, 1989). In particular, Yamagata and Masumoto (1989) demonstrated that the slow oscillations similar to the actual ENSO are reproduced only when the land heating west of the model

ocean is of moderate intensity. Budin and Davey (1989), including a simple atmospheric moist process similar to the one we used in Chapter 2, also shows the three states (perpetual El Niño, perpetual La Niña and oscillatory ones) which depend on the strength of the land heating. In contrast to the scenario put forward by Zebiak and Cane (1987), Schopf and Suarez (1988) and Battisti (1988), reflection of Rossby waves at the western boundary seems to be not involved in the process of model turnabouts.

According to the linear analysis done by Hirst (1988), one might expect oscillations in the Anderson-McCreary type models without land heating. This is certainly not true as Yamagata and Masumoto (1989) has demonstrated. The coupled model eventually settles down into an El Niño state in the case without land heating. Even in the case of weak heating, the oscillations are not generated. In the other extreme of strong heating, the model again does not oscillate but settles down into the other extreme: a La Niña state. Only in the case of moderate heating do we observe oscillations similar to ENSO. The mechanism of the oscillations, however, seems to be totally different from those catalogued so far.

In this chapter, therefore, we investigate the origin of the recurrent air-sea coupled disturbances of Yamagata and Masumoto (1989), i.e. the Anderson-McCreary type model (hereafter referred to as AM-type model), in detail and demonstrate that different air-sea coupled models may give different reasons for ENSO turnabouts. In Section 3.2, the coupled model is described briefly. Section 3.3 is assigned for some model analyses relevant to the origin of the air-sea coupled disturbance. A summary is given in Section 3.4 with some discussions.

3.2 Description of a Coupled Model

3.2.1 Model Atmosphere

The air-sea coupled model used in this chapter is basically the same with the one of AM85 except for some minor changes. The moist process is not included since the structure of the coupled disturbance described in Chapter 2 is similar to that demonstrated

in AM85. Furthermore, the moist process dose not affect the recurrence of the warm coupled disturbance in the AM-type model (Budin and Davey, 1989).

The equations for the atmospheric model are

$$\frac{\partial U}{\partial t} - f V = -\frac{1}{\rho_a a \cos\phi}\frac{\partial p}{\partial \lambda} - \varepsilon U, \tag{1}$$

$$\frac{\partial V}{\partial t} + f U = -\frac{1}{\rho_a a}\frac{\partial p}{\partial \phi} - \varepsilon V, \tag{2}$$

$$\frac{\partial p}{\partial t} + \rho_a C^2 \left(\frac{\partial U}{a \cos\phi \, \partial \lambda} + \frac{\partial V}{a \, \partial \phi}\right) = Q - \gamma p , \tag{3}$$

where (U,V) denote the horizontal velocities, p the pressure perturbation, ρ_a air density, f the Coriolis parameter, and a is the radius of the earth. Variables (λ,ϕ) represent longitude and latitude. The constant ε and γ represent the coefficient for Rayleigh damping and for Newtonian cooling, respectively (both have the value 2.6 per day), and C has the value 60 m/s. With the above parameter values and the prescribed sea surface temperatures as the boundary condition, the model can successfully reproduce the low level wind field in the equatorial region.

3.2.2 Model Ocean

The model ocean is exactly the same with the one in the previous chapter. The equations of the model ocean are

$$\frac{\partial (\mathbf{hu})}{\partial t} + \mathbf{u}.\nabla(\mathbf{hu}) + h\,\mathbf{u}.\nabla\,\mathbf{u} - f\mathbf{k}\times(\mathbf{hu}) = -\nabla\left(\frac{1}{2}\alpha g T h^2\right) + \nu_h \nabla^2(\mathbf{hu}) + \boldsymbol{\tau}, \tag{4}$$

$$\frac{\partial h}{\partial t} + \nabla.(\mathbf{hu}) = \frac{2\delta_o}{h^2 T} - w + \gamma_o\left(\frac{T - T^*}{T}\right), \tag{5}$$

$$\frac{\partial T}{\partial t} + \mathbf{u}.\nabla T = \frac{2}{h}\left(-\gamma_o (T - T^*) - \frac{\delta_o}{h^2}\right) + \nu_h \nabla^2 T, \tag{6}$$

where T is the mixed-layer temperature minus that of the deep layer, h the thickness of the upper layer, **u** the horizontal current velocity vector, τ the wind stress proportional to the wind (U,V), and f, g, t, **k** are the Coriolis parameter, the acceleration due to gravity, the time, and the vertical unit vector, respectively. The values of lateral eddy viscosity ν_h, thermal expansion coefficient α, upwelling velocity from the deep layer w, entrainment coefficient δ_0, thermal relaxation coefficient γ_0 are 5×10^7 cm^2/s, 3×10^{-4} $°C^{-1}$, 16×10^{-5} cm/s, 16×10^4 $cm^3°C/s$ and 12×10^{-4} cm/s, respectively. The reference temperature T^* exactly follows the expression of AM85 such as

$$T^* = 4 + (11.33 - 4) (1 + \cos 2\pi y/y_N) /2, \tag{7}$$

where $y_N = 90^*$ in the present model.

The heating rate Q has the form

$$Q = Q_0 \frac{T - T_c}{\overline{T}(0) - T_c} H(T - T_c), \tag{8}$$

where H denotes the Heaviside step function, $\overline{T}(0)$ the mixed-layer temperature on the equator at a thermodynamic equilibrium state, T_c the critical temperature, and Q_0 is the amplitude factor over the ocean. In contrast to the models used in Chapter 2, the temperature of the deep layer is not necessarily specified with this formulation. We assumed that T_c has the value 8.5°K and Q_0 is 750 cm^2/s^3.

Latent heat release over land (Q_{land}) of which amplitude factor is Q_L is included if necessary as in AM85. This Q_{land} has the form

$$Q_{land} = Q_L X(\lambda) \frac{\overline{T} - T_c}{\overline{T}(0) - T_c} H(\overline{T} - T_c), \tag{9}$$

where

$$X(\lambda) = \exp\,[-\{(\text{ longitude } -140°\text{E}) / 60°\}^2] \quad (\text{for } 0°\text{E} < \lambda < 140°\text{E}) \qquad (10)$$
$$= 0 \qquad (\text{for } \lambda < 0°\text{E},\ 140°\text{E} < \lambda),$$

is a modulation factor.

Some minor changes from the original AM-type model are adopted to have the model more realistic. We used (a) a spherical coordinate system for both atmosphere and ocean, (b) a time-dependent atmosphere instead of a quasi-steady one, (c) values of δ_0, γ_0 and w four times as large as the original values and (d) a heating factor Q_0 1.5 times as large as the original value. The measures (c) and (d) reduce the period of the model ENSO cycles without distorting the physical properties of the original case. The details including definition of various parameters may be found in AM85 and McCreary (1986).

The model ocean covers the area from 50°S to 50°N and from 140°E to 80°W with $1° \times 1°$ resolution, whereas the model atmosphere covers the whole globe between 50°S and 50°N with $2° \times 2°$ resolution. In addition to this standard model, in order to investigate the sensitivity to a longitudinal extent of the model ocean, we utilize another model in which the model ocean has zonal width of 1.5 times as large as the standard one (Figure 1). The informations that are necessary to couple those two components, i.e. oceanic mixed-layer temperature and atmospheric wind stress, are exchanged every 5 model days.

3.3 The Origin of a Model ENSO

Figure 2 shows longitude-time sections of (a) zonal wind velocity, (b) mixed-layer temperature and (c) mixed-layer depth right on the equator for the case with constant external heating $Q_L = 750\ \text{cm}^2/\text{s}^3$ west of the equatorial Pacific (hereafter referred to as the standard run). It is clearly seen that the air-sea coupled disturbance which propagates eastward with a phase speed of 0.18 m/s evolves regularly from the western Pacific. The period of the model ENSO cycle is about 850 days. The structure of the coupled

disturbance is consistent with the one shown in Philander et al.(1984), Yamagata (1985), AM85, Hirst (1986) and others; the atmospheric low pressure center inducing low-level wind convergence is located almost above the thick oceanic mixed-layer associated with the warm mixed-layer temperature. This coherent structure is also similar to the one evolved in a pure form in an aqua-planet (see Chapter 2).

In the case of no land heating, the coupled system settles down into an El Niño state with damped oscillations at an initial stage (Fig. 3). This clearly demonstrates that the unstable U1 mode for Model IV of Hirst (1988) is finally stabilized as the finite amplitude disturbances reach the eastern boundary and affect the basic background state of the oceanic mixed-layer structure. In other words, nonlinearities in the AM-type models dramatically change the state predicted by the linear theory. The external heating, however, can modulate the situation to generate oscillations.

The above shows quite a contrast to the model of Zebiak and Cane (1987), in which the essential processes are linear and nonlinearities act as a bound on the amplitude of the final state of oscillations as in the classical baroclinic instability (cf. Battisti and Hirst 1989). In the present section we clarify a true origin of oscillations in the AM-type models.

3.3.1 Sensitivity to a Longitudinal Extent of the Model Ocean

Longitude-time sections of the mixed-layer depth at different latitudes do not show any signals of long Rossby waves propagating westward as does the one on the equator (Fig. 4). As discussed in Yamagata and Masumoto (1989), the origin of the warm ENSO event in the AM-type model looks very different from other model studies such as Zebiak and Cane (1987), Schopf and Suarez (1988) and Battisti (1988). The most crucial experiment to check whether western boundary reflection of Rossby waves play a major role in generating ENSO cycles will possibly be the one with an ocean of enlarged longitudinal extent (cf. Schopf and Suarez, 1990). We carried out such an experiment in which the model Pacific ocean is made larger zonally by 1.5 times (i.e.

210°) as compared with the standard run (see Fig. 1). If the origin of the warm coupled disturbance is due to western boundary reflection of the off-equatorial Rossby waves somehow related to the previous event, the period of model ENSO cycles must increase. This is simply because the longitudinal distance which the Rossby waves must travel is now longer than that of the standard case. Also, we notice that the period of the oscillation of the U1 mode in Hirst (1988)'s model IV is set by the length of time that the coupled disturbance takes to propagate across the basin.

Figure 5 shows longitude-time sections of (a) zonal wind velocity, (b) mixed-layer temperature and (c) mixed-layer depth on the equator for the present modified run. Quite interestingly, the period of ENSO cycles is exactly the same as the standard case; besides, the strength of the warm coupled disturbance does not change. This demonstrates clearly that the origin of the warm event is not related to western boundary reflection of the Rossby waves excited during the previous event in this model.

One might be tempted to conclude that the results shown here are just consistent with the linear unstable U1 mode of Hirst (1988). This is certainly not true because of several reasons. First, we note that the period of the oscillation of the U1 mode for Hirst (1988)'s model IV is dependent of the basin width. Secondly, Hirst (1988)'s linear analysis should be applied to the case without heating over land. Our final state for the case without land heating is a perpetual El Niño. Nonlinearities thus dramatically change the state predicted by the linear theory. The key area for the origin of the warm coupled disturbance in the AM-type model is in the western Pacific. This is further confirmed by changing the amplitude of land heating.

3.3.2 Sensitivity to an Amplitude Factor of Land Heating

Figure 6 shows the period of oscillations as a function of the amplitude of heating over land (Q_L). When Q_L is small, at most around 100 cm^2/s^3, initial damped oscillations eventually disappear, resulting in a perpetual El Niño. As Q_L increases, the period increases. In particular, the period increases abruptly and the final state is a perpetual La

Niña when Q_L far exceeds 750 cm^2/s^3. For example, in the case with Q_L = 2250 cm^2/s^3 (Fig. 7), the equatorial upwelling excited by the easterly winds associated with the heating is so strong that the coupled disturbance cannot penetrate to the east.

The strong monotonic dependence of the period on the amplitude of heating over land suggests that the origin of the eastward-propagating coupled disturbance may be locked to a certain phase of an oscillatory heating over land. In order to check this idea we have introduced sinusoidal time-dependence into Q_L such as

$$Q_L = 500 + 500 \times \sin (2 \pi t / T) \quad (cm^2/s^3). \tag{3.1}$$

Figure 8 shows the longitude-time sections of atmospheric zonal wind velocity taken from the results for T =360 days and 1000 days. After each maximum of the land heating a solid coupled disturbance evolves in the western tropical Pacific. It is now clearly demonstrated that the origin of the coupled disturbance is regulated by the heating over land in the west. One interesting feature to note for T =1000 days is that a weak coupled disturbance begins to evolve after major disturbance has reached the eastern boundary. However, vigorous return of easterly winds associated with the land heating easily aborts the embryo.

3.3.3 Western Pacific Origin of a Warm Event

Here we discuss in more detail how the coupled disturbance recurs in the western Pacific. For this purpose we examine in detail one complete cycle from day 1800 through day 2800 of the standard run. This period covers from a state in which a coupled disturbance begins to move eastward to a state in which another new coupled disturbance evolves in the western Pacific (see Fig.2).

Figure 9 shows the time series of zonal wind, zonal current, mixed-layer temperature and mixed-layer depth averaged over the western Pacific from 145°E to 165°E and from 5°S to 5°N. The variation of mixed-layer depth and mixed-layer

temperature is almost in phase as in AM85. This is because the mixed-layer temperature of the AM-type model is determined mainly by entrainment depending only on the mixed-layer depth. The averaged zonal current is always eastward. However, it is accelerated (decelerated) during the period when the wind is westerly (easterly). The wind reversal from westerly (easterly) to easterly (westerly) occurs at about day 2150 (day 2530). As the eastward current increases (decreases), the mixed-layer depth decreases (increases). The cause is discussed shortly in the next paragraph.

Figure 10 shows the time series of zonal mass transport across three different spans (5°S - 5°N, 5°N - 15°N and 15°N - 25°N) on the meridian of 165°E . Mass transport across the off-equatorial sections shows only small changes. In particular, the westward transport across the subtropical section (15°N - 25°N) is almost constant during the period. However, there is an extremely large transport variation across the tropical section (5°S - 5°N). It can be seen that the eastward transport decreases a lot and even reverses the direction when the coupled disturbance moves eastward leaving the western Pacific (from about day 2100 to about day 2500). As the next coupled disturbance evolves in the western Pacific, the eastward transport revives rather strongly (after day 2500). All those transport changes are directly related to the wind direction above the equatorial western Pacific (cf. Fig. 9). Although there is a northward leakage across 25°N between the western boundary and 165°E, those transport is almost constant during the period (Fig. 11). Therefore, the main part of the constant westward transport across the subtropical section converges rather regularly into the tropical region along the western boundary. The decrease of the eastward mass transport across the tropical section means that the water mass accumulates in the equatorial western Pacific (see Fig. 9).

Figure 12 shows horizontal distributions of (a) oceanic mixed-layer depth, (b) mixed-layer temperature, (c) current vector sticks and (d) zonal wind at about day 2100. It should be noted that the warm coupled disturbance evolved in the western Pacific moved eastward and reached near the dateline at this time. The off-equatorial easterly

wind associated with the land heating generate the westward currents in the western Pacific with maxima near 20°N and 20°S. These currents show small temporal changes (Fig.10) and converge into the equatorial region along the western boundary. It is important to note here that the mixed layer depth must decrease in the offshore direction (eastward) because of the geostrophy of the western boundary current. The equatorial eastward current in the western Pacific, which has been accelerated by the westerly wind associated with the coupled disturbance, reaches the maximum at this time. Thus the water mass in the western tropical Pacific is transported eastward excessively so that the mixed-layer depth becomes shallow with cool water temperature.

As the coupled disturbance moves farther eastward (Fig.13), there is room for the easterly associated with the heating over land to prevail in the equatorial western Pacific. This easterly decelerates the eastward equatorial current. The equatorward mass flux along the western boundary, however, remains almost the same and thus the water mass accumulates in the equatorial western Pacific. This, in turn, leads to increase of mixed-layer temperature as a result of the reduction of cold water entrainment from below. The low-level wind convergence is then further strengthened above the warm region and increases both of the area and the temperature of the warm mixed-layer. Since the geostrophy of the equatorward western boundary current demands that the mixed-layer depth should decrease eastward very near the western boundary, the warm pool has its temperature maximum farther eastward.

The above positive air-sea-land feedback process is a prerequisite for the birth of the air-sea coupled disturbance in the present AM-type model. As both of the area and the temperature of the warm mixed-layer increases, weak westerly winds associated with the maximum atmospheric heating appear in the equatorial western Pacific (cf. Gill, 1980). These winds have a positive correlation with eastward currents and thus satisfy the necessary condition for the growth of the air-sea coupled disturbance (cf. Yamagata, 1985). As the coupled disturbance grows, it moves eastward as demonstrated in Philander et al. (1984) and in Chapter 2.

3.4 Conclusions and Discussion for Chapter 3

In this chapter, the origin of the warm coupled disturbance in the AM-type model is investigated in detail. It is shown that the period of the model ENSO does not depend on the longitudinal extent of the ocean but on the amplitude of the heating over land in the west. This means that western boundary reflection of off-equatorial oceanic Rossby waves generated in the previous ENSO event are not responsible for the origin of the following event. The origin of the coupled disturbance in the present model may be summarized as follows. The heating over land excites easterly winds with a large meridional extent in the model western Pacific. Those easterly winds always generate the westward oceanic flow in the off-equatorial region. The mass flux associated with this westward flow converges into the equatorial region along the western boundary. The eastward flow along the equator is reduced by the revived easterly winds after the westerly region associated with the coupled disturbance of the previous event moves far eastward. This leads to the accumulation of warm water in the equatorial western Pacific and provides the deep and warm mixed-layer. As a result of the increased mixed-layer temperature, the low-level wind convergence is strengthened above the region. The resultant positive air-sea-land feedback results in evolution of the coupled disturbance in the western Pacific. Only when the intensity of the land heating is of moderate intensity can the coupled disturbance move eastward and give rise to oscillations. This is because oceanic cooling in the central Pacific, associated with upwelling due to the winds, is too weak to prevent the eastward movement of the coupled disturbance. In the extreme of weak heating over land, however, the warm water accumulation is too weak to generate another coupled disturbance, once the model has settled down into the El Niño state.

The above new scenario for the origin of the warm coupled disturbance is very different from those described in Battisti (1988), Schopf and Suarez (1988) and Zebiak and Cane (1987). In those models, the western boundary reflection of off-equatorial oceanic Rossby waves excited during a cold event plays a crucial role in triggering the

following warm coupled disturbance. In the present AM-type model, however, oceanic Rossby waves are highly damped due to the same ocean-atmosphere interaction that gives rise to the air-sea coupled disturbance (Yamagata, 1985; 1986). This is why the Rossby waves does not come into play in the AM-type model. The heating over land in the west regulates the phenomena and causes a transition between two equilibria, that is, La Niña and El Niño.

As discussed in Yamagata (1985, 1986) and Hirst (1986), the above mechanism is very sensitive to amplitudes of ocean-atmosphere coupling parameters as well as processes which determine atmospheric heating and SST. For example, Wakata and Sarachik (1990) has recently shown that two stationary unstable modes which do not oscillate exist when the product of two ocean-atmosphere coupling coefficients exceeds a certain critical value. The two stationary modes correspond to La Niña state and El Niño state respectively. Actually, our corresponding key parameter is approximately 10 times larger than the critical value calculated by Wakata and Sarachik (1990). This suggests that we have treated a case with rather strong ocean-atmosphere coupling. It should be noticed, however, that the key parameter is very sensitive to the choice of the oceanic long wave speed c_o. In the present model c_o = 1.71 m/s, whereas Zebiak and Cane (1987) adopted c_o = 2.9 m/s. A precise estimation of the oceanic long wave speed as well as ways of coupling is thus very important in modelling ocean-atmosphere interaction.

Yasunari (1991) has found a high positive correlation between the warm (cold) SST-OHC anomaly in the western Pacific in the winter before the mature ENSO year, and heavy (light) rainfall over India during the preceding summer. This suggests that the strong biennial oscillation (BO) of the Asian Summer Monsoon, i.e. the air-sea-land process, plays an important role in determining ENSO cycles (cf. Meehl, 1987). Barnett et al.(1989) also suggests a possibility of a snow-monsoon-El Niño connection using a coupled General Circulation Model; anomalous land processes over Asia can cause anomalous SSTs in the equatorial Pacific. The present model result, which stresses the

importance of land heating west of the Pacific ocean in the origin of the ENSO cycles of the AM-type models, seems to be consistent with those arguments.

The above air-sea-land process may determine not only the anomalous condition in the equatorial Pacific but also the basic background state in the western tropical Pacific. Meehl (1987) suggested that the Asian monsoon plays an important role in the dynamically coupled atmosphere-ocean system in the Indian-Pacific region and that the onset of the warm ENSO event is affected by its seasonal and interannual variabilities. Therefore, it is of interest to know the mechanisms that determine the mean condition and its seasonal cycle there. In the next chapter, we will clarify seasonal cycle of the western tropical Pacific as response to the Asian monsoonal winds.

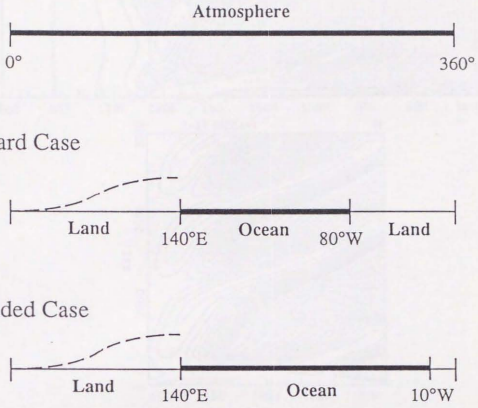

Fig.1. A schematic diagram showing the location of the land (thin solid lines) and the ocean (thick solid lines). The atmosphere has cyclic boundary conditions in both cases. Convection is fixed over the land west of the model oceans, and dashed curves illustrate distribution of it.

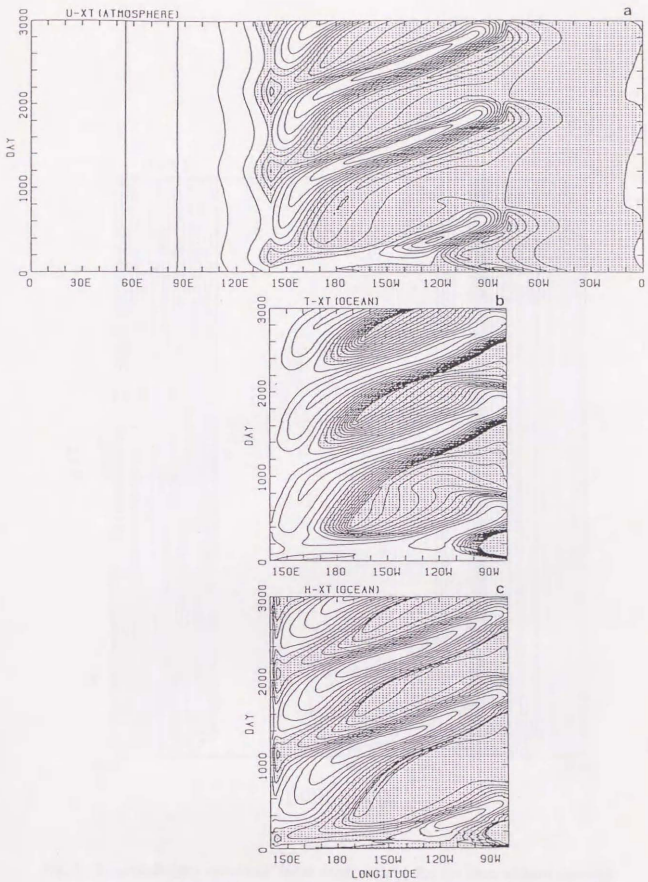

Fig.2. Longitude-time sections of (a) zonal wind velocity, (b) mixed-layer temperature and (c) mixed-layer depth right on the equator for the standard run. Contour intervals are 2 m/s, 0.5 °C and 10 m, respectively. Regions of the mixed-layer less than 8.5°C or 100m and those of easterly winds are shaded.

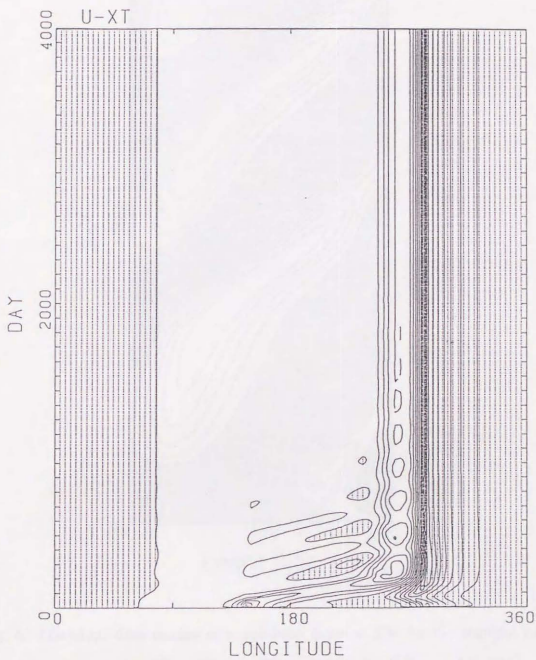

Fig. 3. Longitude-time section of zonal wind velocity for the case without external heating. Contour interval is 2 m/s.

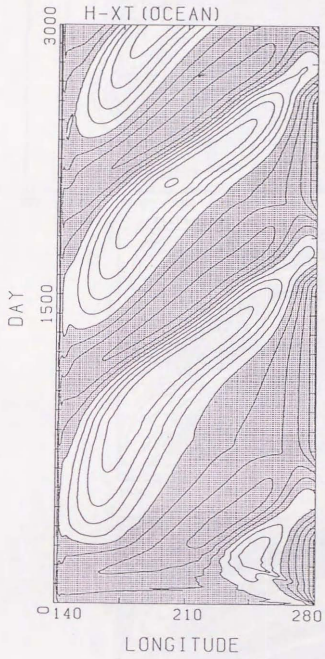

Fig. 4. Longitude-time section of mixed-layer depth at 5°N for the standard run. Contour interval is 10m. Regions of the mixed-layer shallower than 100m are shaded.

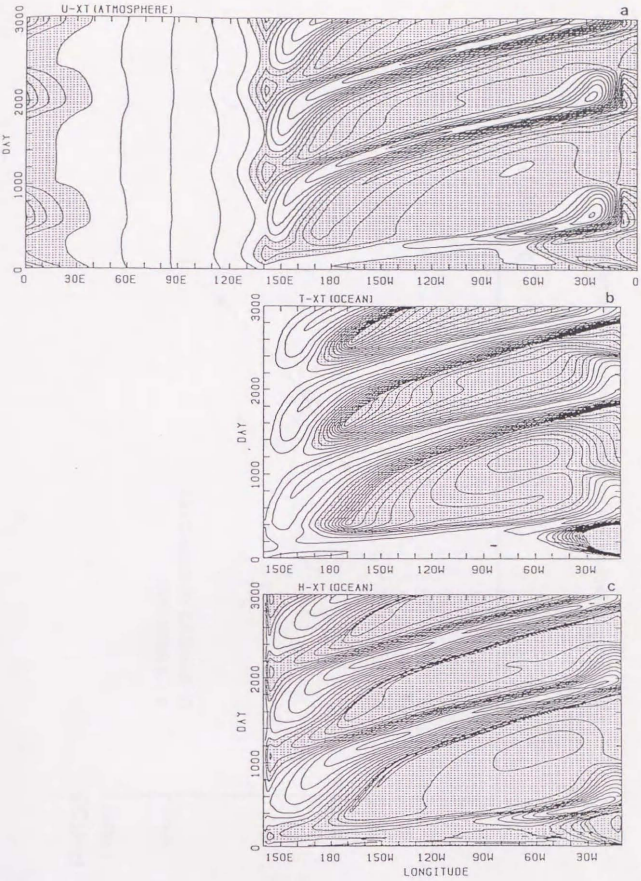

Fig. 5. As in Fig.2 but for the modified run with the expanded model Pacific.

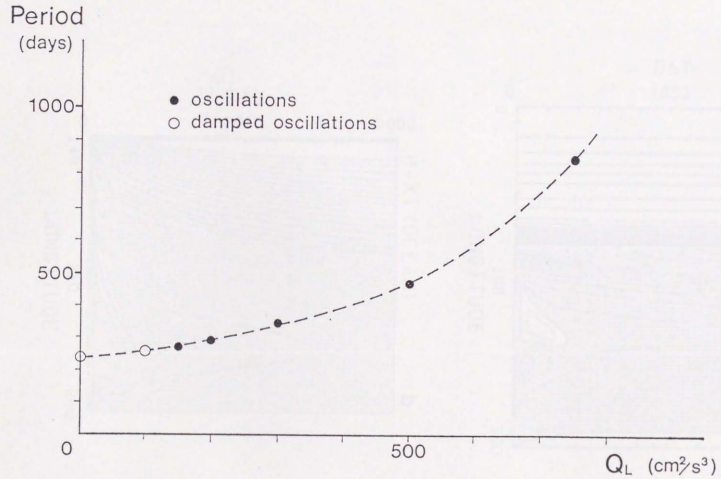

Fig. 6. Period of oscillations as a function of the amplitude of land heating.

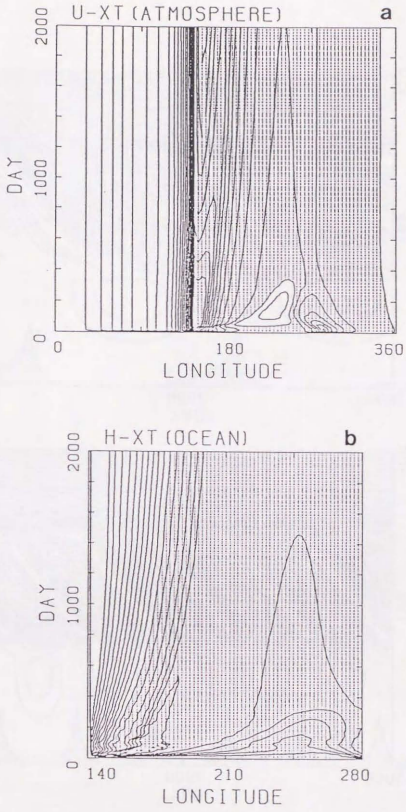

Fig.7. Longitude-time sections of (a) zonal wind velocity and (b) mixed-layer depth right on the equator for the case of Q_L = 2250 cm^2/s^3. Contour intervals are 2 m/s and 10 m, respectively. Regions of the mixed-layer less than 100m and those of easterly winds are shaded.

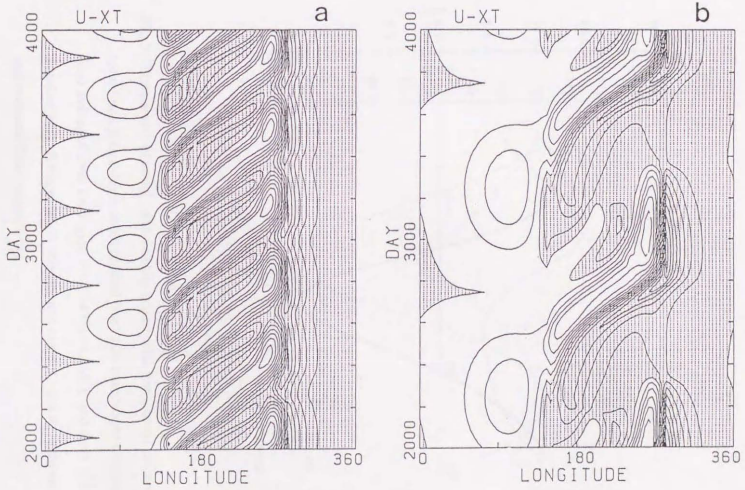

Fig. 8. As in Fig. 2(a) but for the case with oscillatory heating over land. a) Period is 360 days. b) Period is 1000 days.

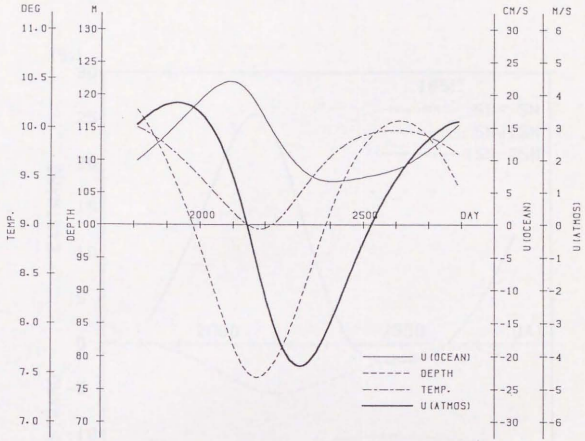

Fig.9. Time series of zonal wind velocity (thick solid line), zonal current velocity (thin solid line), mixed-layer depth (dashed line) and mixed-layer temperature (dash-dot line) averaged over the region from 145°E to 165°E and from 5°S to 5°N for the standard run. Positive wind velocity and current velocity indicate westerly wind and eastward flow, respectively.

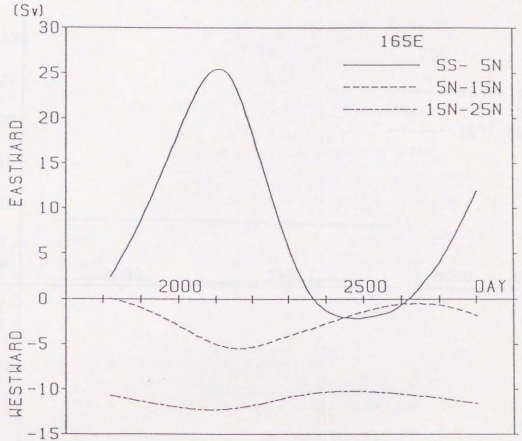

Fig.10. Time series of zonal mass transports across three different spans (5°S - 5°N, 5°N - 15°N and 15°N - 25°N) on the meridian of 165°E.

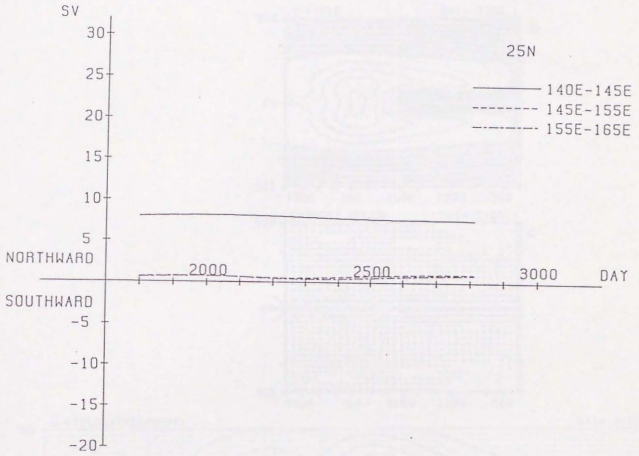

Fig.11. Time series of meridional mass transports at 25°N across three different spans (140°E - 145°E, 145°E - 155°E and 155°E - 165°E).

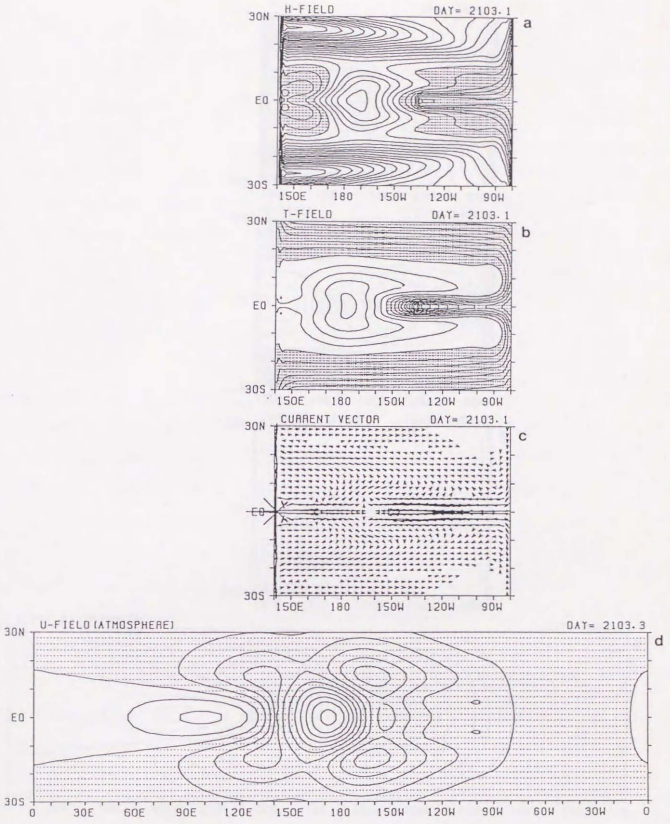

Fig.12. Horizontal distributions of (a) oceanic mixed-layer depth, (b) mixed-layer temperature, (c) current vector sticks and (d) zonal wind velocity at about day 2100. Contour intervals are 10 m, 0.5 °C and 2 m/s. Regions of the mixed-layer less than 8.5°C and 100m, and those of easterly winds are shaded.

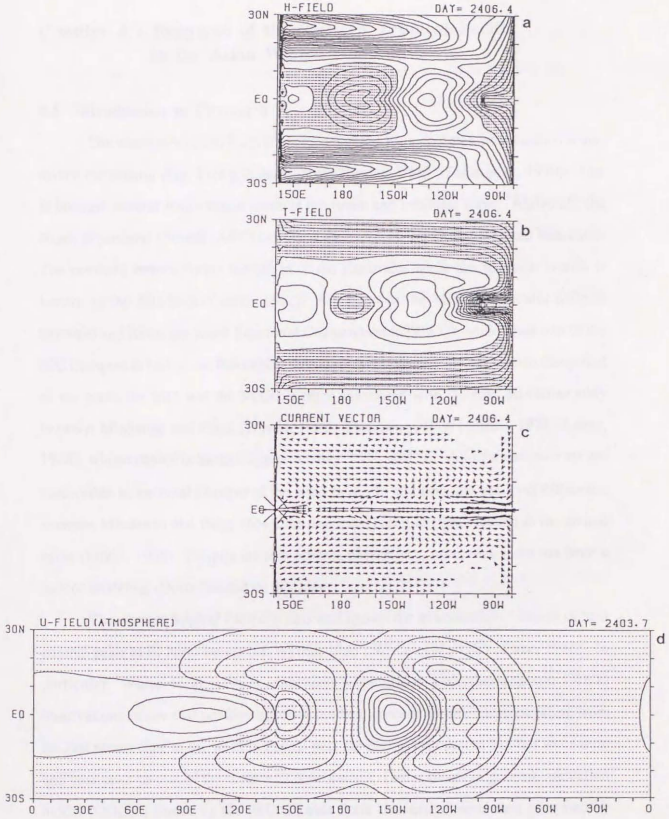

Fig.13. As in Fig.12 but for about day 2400.

Chapter 4 : Response of the Western Tropical Pacific to the Asian Winter Monsoon

4.1 Introduction to Chapter 4

The western tropical Pacific is characterized by a complex near-surface wind-driven circulation (Fig. 1) (e.g. Schott, 1939 ; Kendall, 1989 ; Toole et al., 1990). This is because several major ocean currents terminate and originate there. Above all, the North Equatorial Current (NEC) intersects the coast of the Philippines and bifurcates. The northern branch forms the origin of the Kuroshio, while the southern branch is known as the Mindanao Current (MC). A portion of the MC subsequently deflects eastward and forms the North Equatorial Countercurrent (NECC), while some part of the MC transport is lost to the Indonesian throughflow. The cyclonic circulation composed of the NEC, the MC, and the NECC is often associated with the cold Mindanao eddy between Mindanao and Palau (Wyrtki, 1961 ; Masuzawa, 1968 ; Nitani, 1972 ; Lukas, 1988), whose center is located approximately 7 °N, 130 °E. All of those currents are susceptible to seasonal changes of the wind field. In addition, the sea level difference between Mindanao and Palau shows the dominant biennial signal locked to the annual cycle (Lukas, 1988). Despite the rich oceanic phenomena, up to now there has been a lack of modeling efforts focused on this area.

The western tropical Pacific is also well known for its anomalous increase of heat content prior to El Niño events (cf. Wyrtki, 1985 ; White et al., 1985 ; Cane, 1986). In particular, White et al. (1987), analyzing expendable bathythermograph (XBT) observations, show that positive upper-ocean heat content anomalies propagating from the east accumulate in the western Pacific near the Philippine coast in late fall and winter one year prior to that of the mature El Niño events. Using an ocean general circulation model (OGCM) forced by the FSU (Florida State University) wind data compiled by Goldenberg and O'Brien (1981), Takeuchi (1989) confirmed that all El Niño events from 1969 through 1984 were preceded by positive surface dynamic height anomalies in the western Pacific near the Philippine coast (see also Kitamura, 1990). Figure 2 shows

those anomalies with a significant biennial oscillation actually observed along 137°E by Japan Meteorological Agency. We notice here that the oceanic heat content anomaly corresponds well with the sea surface temperature (SST) anomaly even in the western tropical Pacific, which is characterized by the thick thermocline compared to the central or eastern tropical Pacific. This remarkable relation suggests that the oceanic heat content anomaly in the western tropical Pacific may influence atmospheric conditions and, hence, the generation of the atmosphere-ocean coupled disturbances associated with the El Niño/Southern Oscillation (ENSO) phenomenon (see Chapter 3).

In order to gain an insight into the mechanism of the biennial oscillation locked to the annual cycle in the western tropical Pacific and of the precondition of the El Niño events, it will be useful to investigate the seasonal evolution of the oceanic conditions around the Mindanao eddy, as implied by Philander et al. (1987b). Therefore, in this chapter, we focus our attention on seasonal variations of the western reaches of the Pacific using a OGCM adapted from the GFDL (Geophysical Fluid Dynamics Laboratory/NOAA) model.

4.2 Model Description

The basic physics contained in the model are almost the same as that of Philander et al.(1987b), except for resolving rather realistic geometry (cf. Bryan, 1969 ; Cox, 1984). The model equations are described in detail in Appendix. Here we briefly summarize our model parameters. Our model covers the Pacific and Indian oceans and extends from 30°S to 50°N in latitude (Fig. 3). The horizontal model grid resolution is 0.5° in both longitudinal and latitudinal direction. There are 11 levels in the vertical with 5 levels in the top 110m in order to focus on the variabilities in the upper few hundred meters (Fig. 4). The actual topographic and geometrical data supplied by GFDL are fitted in the model. Along the lateral boundary, we apply a no-slip condition. The bottom boundary is, however, slippery. The coefficient of lateral eddy viscosity is 2×10^7 cm^2/s, whereas the coefficient of lateral eddy diffusivity is 1×10^7 cm^2/s. Because of the spatial

resolution the magnitude of the lateral eddy viscosity is twice as large as that of Philander et al. (1987b). Near the southern and northern boundaries (poleward of 25°S and 45°N), the values of these coefficients are increased to values twenty times as large as the inner ones. The temperatures are relaxed to the Levitus (1982) seasonal climatology within the sponge layer so that artificial wall effects are weakened. The vertical eddy viscosity and diffusivity are based on the formulae given by Pacanowski and Philander (1981).

The heat flux across the ocean surface is:

$$Q = SW - LW - QS - QE, \tag{1}$$

where the solar shortwave heating (SW) is assumed to take the constant value of 242 W/m^2 within 20° latitude band and decreases linearly to 126 W/m^2 between 20° and 50° latitude. The long wave back radiation (LW) has the constant value of 55.7 W/m^2. The sensible heat flux (QS) is given by the formula:

$$QS = \rho_A C_D C_p V(T_o - T_A), \tag{2}$$

and the latent heat flux due to evaporation (QE) is given by

$$QE = \rho_A C_D L V[e_s(T_o) - \gamma e_s(T_A)]\ (0.622/p_A), \tag{3}$$

where air density $\rho_A = 1.2\times10^{-3}$ g/cm^3; atmospheric pressure p_A =1013 mb; latent heat of condensation $L = 2.49\times10^3$ J/g; drag coefficient $C_D = 1.4\times10^{-3}$; specific heat C_p =1.0 J/gK; T_o is the sea surface temperature; T_A is the atmospheric temperature at the surface; V is the surface wind speed; and γ is the relative humidity, assumed to be 0.8. The saturated vapor pressure e_s is given by

$$e_s(T) = 10^{[9.4051-(2353/T)]}. \quad (4)$$

No measures were taken for cloudiness and, following Philander and Seigel (1985), T_A is always assumed to be 1.5°C less than the predicted sea surface temperatures. Also the surface wind speed in the formulae QS and QE is assumed to be more than or equal to 4.8 m/s so that the effect of high-frequency wind fluctuations that are absent from the mean monthly winds is taken into account.

The initial condition is the climatological winter mean of the temperature field (Levitus, 1982). Monthly mean climatological winds (a revised version of Hellerman and Rosenstein, 1983) drive the model for four years (Fig. 5)[1] . The results discussed in later sections are taken from the final fourth year since they have approximately reached the dynamical equilibrium.

4.3 Seasonal Cycle of the Western Tropical Pacific

4.3.1 Surface Currents and temperatures

Figure 6 shows the annual march of surface currents (at a depth of 10 m) simulated in the present model. Seasonal transport variations of the major modeled currents in the western tropical Pacific are shown in Figs. 7 and 8. As depicted in Section 4.1, the NEC strikes the coast of the Philippines and always bifurcates at a latitude around 13°N. The northern branch constitutes the origin of the Kuroshio, while the southern branch is the MC along the Philippine coast. It should be noted that much more of the NEC flows into the Kuroshio than into the MC (cf. Whitehead, 1985). The above bifurcation latitude is consistent with the observational evidence (Nitani, 1972 ; Kendall, 1989 ; Toole et al., 1990).

It is seen in Fig. 7 that both NEC and NECC across 130°E are intensified from late fall through spring in accordance with the active northeast trade winds with strong

[1] The winds compiled by Florida State University (cf. Goldenberg and O'Brien, 1981) have also been used. The result is almost the same as the one reported here.

cyclonic curl (cf. Fig. 5). This reflects on the southward transport of the MC across 8°N and the northward transport of the Kuroshio across 18°N (Fig. 8). Transport variations of both NEC and NECC across 160°E are different from those across 130°E. In particular, the two currents across 160°E have the minimum transport in spring (Fig. 7). This is consistent with the existence of a recirculating cyclonic gyre west of 160°E in winter and spring, as demonstrated in Figure 6. The western limb of this gyre constitutes the MC. This is why the transport of the MC shows a maximum in winter (Fig. 8). Hereafter we call the recirculating gyre the Mindanao Dome. The Mindanao Dome covers an area much larger than the Mindanao eddy described in Section 4.1. The eastern edge of the Mindanao Dome (around 150°E in winter) is associated with a rather broad northward flow (Fig. 6). This northward flow has multiple origins in the model and partly connects with the currents off New Guinea.

We note here that the surfaced New Guinea Coastal Undercurrent (NGCUC), or the New Guinea Monsoon Current, in summer and fall is well resolved along the northern coast of New Guinea in Fig. 6 (cf. Schott, 1939 ; Tsuchiya et al., 1989). This surfaced NGCUC intersects Halmahera Island right on the equator and generates the anticyclonic Halmahera eddy with a damped lee-wave pattern east of the island, as observed using drifters during the Western Equatorial Pacific Ocean Circulation Study (WEPOCS) (Hacker et al., 1989). Since our old model without Halmahera Island could not resolve the Halmahera eddy, we may conclude that the small Halmahera Island is responsible for the existence of the Halmahera eddy. The northern rim of this Halmahera eddy constitutes the NECC.

In winter, the New Guinea Coastal Current flows only along the coast of Papua New Guinea and deflects eastward when it reaches the equator, as observed by Lindstrom et al. (1987). The resultant eastward equatorial surface current east of 140°E is consistent with the local eastward winds at that time, as pointed out by Philander et al. (1987b). The eastward equatorial surface current is then blocked near 150°E by the revived South Equatorial Current (SEC) in spring and partly deflects northward, flowing

along the eastern flank of the Mindanao Dome. This northward flow joins eventually with the NEC. Some drifters released off New Guinea during the WEPOCS actually took the above route (Wooding et al., 1990).

Figure 9 shows the surface temperatures at a depth of 10m. It is not easy to detect a simple relation to the complex surface currents. However, it is clearly seen that the warm water shows strong annual fluctuations. In particular, it stretches far into the north in September. In March it retreats to the southernmost position.

4.3.2 Subsurface currents and temperatures

Figures 10 and 11 show the annual march of the subsurface currents and temperatures at a depth of 100 m. We again find that the cold Mindanao Dome is composed of the NEC in the northern flank, the MC in the western flank, and the NECC in the southern flank (Fig. 10). The NECC deflects northward near the eastern edge of the dome at around 140°E in winter as depicted in the previous subsection. The cold core of the dome expands southeastward during winter with intensifying the NECC (Fig. 11), whereas warm water forming a ridge intrudes along the southern flank (near 4°N) of the cold dome in late spring. This warm water gradually erodes the cold dome. The dome, however, starts evolving again in late fall off the Philippine coast.

The NGCUC is a permanent feature at a depth of 100 m even during the northwest monsoon in austral summer. A portion of the NGCUC turns east when it crosses the equator and becomes a source of the Equatorial Undercurrent (EUC) as described by Tsuchiya et al. (1989). The EUC develops only east of 140°E from June through November. In winter and spring the NGCUC crosses the equator and joins in the NECC along the southern flank of the Mindanao Dome.

4.3.3 Meridional heat transport associated with the Mindanao Current

Figure 12 shows simulated meridional heat transport across 8°N in the Pacific with contributions from the MC (between the Philippine coast and 130°E) and the Ekman

transport (between 130°E and the American coast). Southward heat transport associated with the MC (above a depth of 310m) varies from its minimum 0.27×10^{15} W in May to its maximum 1.11×10^{15} W in November in accordance with the variation of mass transport. Since the northward Ekman flux carries a significant amount of heat to the north in the central Pacific due to the strong northeasterly wind in winter, the MC plays a minor role in the net meridional heat transport. However, as suggested by Philander et al.(1987b), the relative contribution increases from July through October. This is because the Ekman flux is extremely suppressed in the central Pacific due to the northward migration of the ITCZ in the boreal summer.

4.3.4 Heat budgets off the Philippine coast

It is of interest to analyze a heat budget in the dome region to understand a mechanism at work. In order to calculate the heat budgets in different seasons, we consider three artificial boxes (A, B and C) in the upper 110 m off the Philippine coast. Box A has a rectangular domain bounded by latitudes (5 °N, 10 °N) and longitudes (127 °E, 135 °E), which cover the core part of the Mindanao Dome. Box B next to Box A is also rectangular bounded by latitudes (5 °N, 10 °N) and longitudes (135 °E 145 °E). This box is located in the eastern half of the Mindanao Dome when it reaches the peak of its activity in winter. Box C next to Box B is bounded by latitudes (5 °N, 10 °N) and longitudes (145 °E, 155 °E). Box C is located at the eastern edge of the Mindanao Dome. The results are shown in Fig. 13.

The rate of the heat storage in Box A is negative from October through March (Fig.13(a)). In particular, the averaged temperature drops most sharply in January at a rate of -0.64° per month. The cooling is due to the divergence of the heat transport. More specifically, it is due to upwelling of cold subsurface water (Fig.13(b)). This model upwelling from fall through winter is well explained by the cyclonic local wind-stress curl associated with the Asian winter monsoon. Therefore, the core of the model's Mindanao Dome is generated by the local wind-stress curl of the Asian winter monsoon

(see Fig. 5). In spring and early summer, the averaged temperature increases mainly due to convergence of the heat transport (adiabatic process) and partly due to increased surface heat flux (diabatic process). The downwelling in spring and early summer cannot be due to local wind stress since the wind still favors upwelling. It must be due to propagation of warm water generated remotely. As seen in Fig. 11, the warm water actually propagates into the domain from the east.

The temperature averaged within Box B begins to drop in October and reaches the maximum cooling rate -0.75° per month in December (Fig.13(c)). The cooling is due to the divergence of the heat transport as is the case for Box A. However, the upwelling is very weak here in contrast to Box A (Fig.13(d)). This means that the cold water upwelled remotely in the west progresses eastward and enters into Box B, as seen in Fig. 11. The averaged temperature begins to rise in March and the heating rate reaches the maximum at 0.46° per month in April. Although the winds favor upwelling almost all year around, the model vertical velocity shows active downwelling in the spring and early summer. Therefore the heating is due to the lateral convergence of the heat transport, i.e. propagation of warm water generated remotely, as in Box A.

The averaged temperature in Box C also drops sharply in December (Fig.13(e)). However, the winds only induce very weak upwelling (Fig.13(f)). The major contributions come from both lateral divergence and surface fluxes (mainly due to the effect of evaporation enhanced by strong northeast trade winds). The temperature begins to increase in February, and the rate reaches the maximum in May when the surface flux changes the sign. This heating is due partly to the local anticyclonic wind stress curl, which induces downwelling, and partly to the lateral convergence of the heat transport, of which the major portion, however, is used to cancel the active cooling by the surface fluxes.

One aspect to be noticed here is that the heat storage in each box is monotonically decreasing even during the fourth year, as seen by integrating the solid curve of the rate of change of heat storage for 12 months. The average temperature decreases during the

fourth year are 0.56 °C, 0.85 °C, and 1.05 °C for Box A, B, and C, respectively. This climate drift on the absolute value of the temperature is due to the fact that the density field initialized with the Levitus climatology has not yet reached a thermal steady state under the present formulation of surface fluxes. Since we observe the worst situation in Box C where the seasonal diabatic process cannot be negligible, the formulation itself needs to be improved. However, we reasonably expect that the major results presented here will not be seriously affected by the slow climate drift. This is because the seasonal evolution of the dome is mainly dominated by the quick adiabatic processes in which the currents and temperature gradients are in equilibrium (cf. Philander et al., 1987a).

Summing up the above results, the model's Mindanao Dome is generated off the Philippine coast during fall and winter due to cold water upwelling induced by local wind-stress curl associated with the Asian winter monsoon. It expands eastward with the NECC at the southern edge of the cold dome and reaches the maximum in late winter. From early spring through early summer, the dome weakens mainly due to intrusion of warm water from the east. This warm water is generated in winter by the northeast trade winds in the western Pacific near 160°E. The longitude-time diagram of the heat content anomaly at 5°N (Fig. 14) clearly demonstrates the above evolution of the Mindanao Dome.

The warm anomaly propagates to the west at about 0.3 to 0.4 m/s in our model, which is consistent with the phase speed of a first baroclinic mode of equatorial long Rossby waves used in other model studies (cf. Busalacchi et al., 1983 ; Kubota and O'Brien, 1988). Mitchum and Lukas (1990), using sea level data at seven island stations, show that the annual cycle in the same region propagates towards the west at about 0.5 m/s, somewhat higher than the above speed.

4.3.5 Controlled experiments on the evolution of the Mindanao Dome

In order to further confirm the Mindanao Dome evolution, we held the winds constant from 15 September onward for ten months. This first control run (CR 1) does

not show any dome evolution (Fig. 15). Figure 14, however, demonstrates that the seasonal response of the Pacific west of 170°E is very different from the other part. It looks as if there were a node near the meridian. This suggests another control run (CR 2) in which the seasonal change of the winds is assumed only west of 170°E. East of the date line, we have kept the winds constant from 15 September for ten months. The magnitude of the seasonal wind variation has been linearly increased up to the actual value from the date line through 170°E. The result of CR 2 is shown in Figure 16. As expected, the evolution of the model's Mindanao Dome is almost perfectly simulated by the seasonal wind variations west of 170°E. It is more clearly demonstrated in Figure 17, in which we show the time evolution of spatial correlation coefficients of heat content anomaly between the standard run and each of the control runs. The domain of calculation is (5°S - 20°N, 125°E - 160°E). The first control run loses correlation almost completely with the standard run five months after the surgery of the wind field, whereas CR 2 maintains high correlation (> 0.8) with the standard run for at least ten successive months. In particular, the correlation is almost perfect for five months up to February.

4.4 Conclusions and discussion for Chapter 4

Seasonal variations of the western tropical Pacific is investigated in this chapter in terms of the response to the Asian monsoon winds. It is found that the model's Mindanao Dome evolves in late fall off the Philippine coast due to local upwelling as a positive curl of the Asian winter monsoon winds increases over the region. It expands eastward with a recirculation composed of the North Equatorial Current in the north, the Mindanao Current in the west, and the North Equatorial Countercurrent in the south. After reaching a maximum in winter, it begins to decay in spring in accordance with a retreat of the local positive wind-stress curl. The decaying process is accelerated due to intrusion of the downwelling Rossby waves excited in winter by the northeast trade winds farther eastward near 160°E. In other words, as additional controlled experiments

demonstrated, the evolution of the model's Mindanao Dome is almost perfectly determined by the seasonal wind variations west of 170°E.

A corollary is that interannual modulations of the annual cycle of wind in the western Pacific may cause the interannual variations of the Mindanao Dome and the oceanic heat content anomaly off the Philippine coast. Figure 18 shows composite FSU wind-stress anomalies classified into warm and cold winters. When the average winter sea surface temperature around Japan is warmer than normal, the winter is assigned into the warm winter set and vice versa (cf. Hanawa et al., 1989). The warm winters basically correspond to the mature phase of El Niño years. Therefore, it is colder than normal in the western tropical Pacific. It is clearly seen that, during the warm (cold) winter, the northeast winter monsoon winds off the Philippine coast are weaker (stronger) than normal, whereas the northeast trade winds near 160°E are stronger (weaker) than normal. According to the present simulation, both effects will possibly contribute to immaturity (maturity) of the Mindanao Dome, thus, giving rise to a negative feedback mechanism on seawater temperatures in the western tropical Pacific. This hypothesis must be checked further by research.

The possible interaction between the winter Asian monsoon and the seawater temperature anomaly in the western Pacific appears to be the origin of the biennial oscillation of the heat content anomaly in the western Pacific, and also to relate to the precondition of the air-sea coupled disturbances associated with the El Niño events. The present study suggests that the Asian monsoon system, i.e. the air-sea-land system in the western tropical Pacific, may strongly regulate oceanic conditions both seasonally and interannually in the tropical Pacific west of the date line (cf. Yamagata and Masumoto, 1989; Yasunari, 1991).

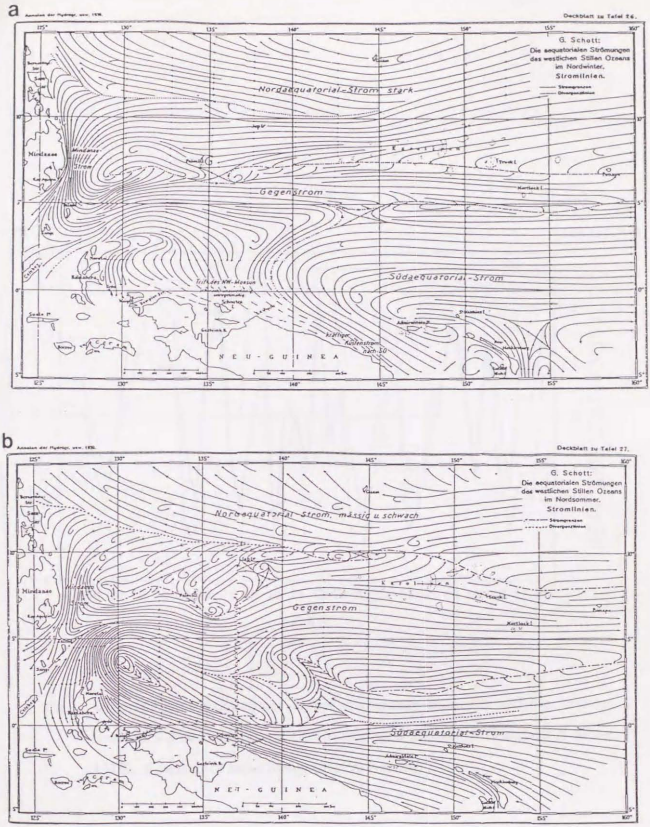

Fig 1. Surface currents of the western tropical Pacific Ocean. a) boreal winter and b) boreal summer. (After Schott, 1939)

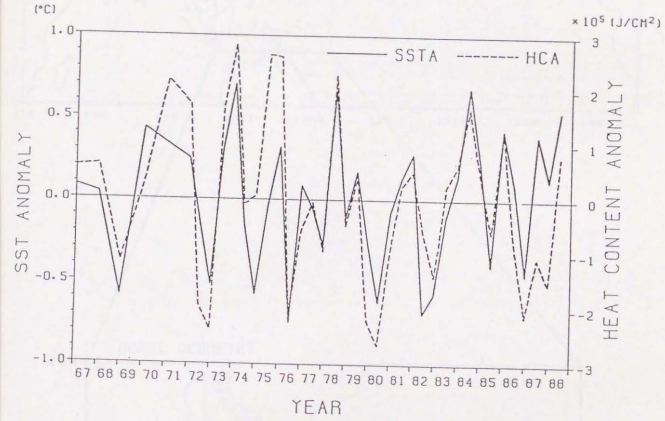

Fig.2. Observed time series of sea surface temperature anomalies and heat content anomalies (above a depth of 300m) averaged between 2°N and 10°N along 137°E. (Courtesy of Japan Meteorological Agency)

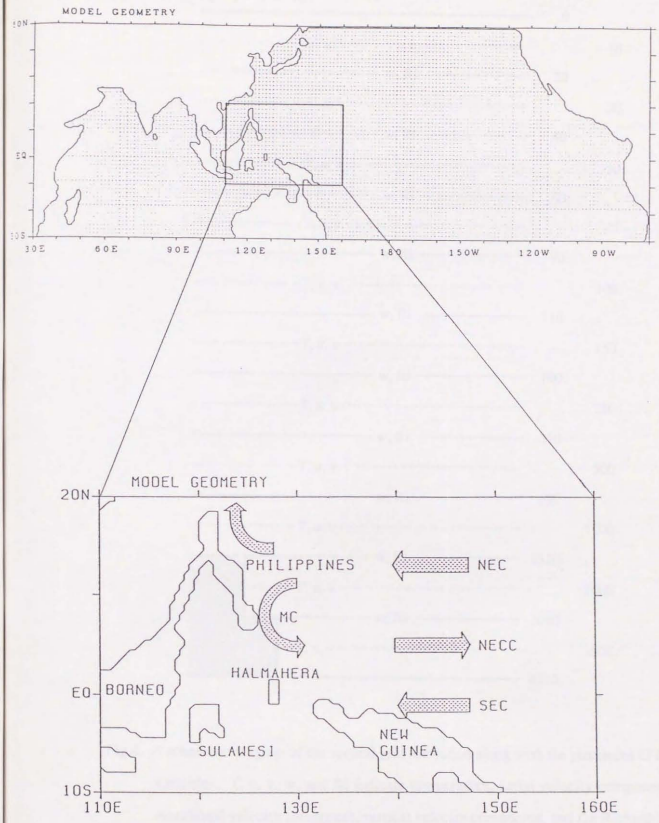

Fig.3. Model geometry and enlarged map of the western Pacific region with a schematic diagram of the horizontal surface circulation.

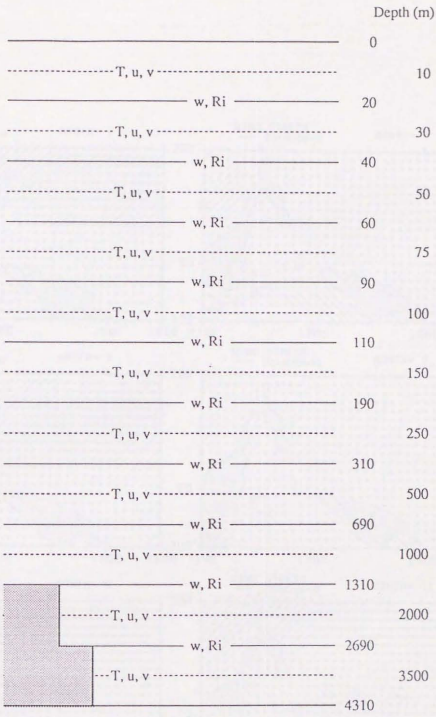

Fig.4. A schematic diagram of the vertical grid resolution along with the placement of the variables. T, u, v, w, and Ri indicate temperature, zonal velocity component, meridional velocity component, vertical velocity component, and the Richardson number, respectively.

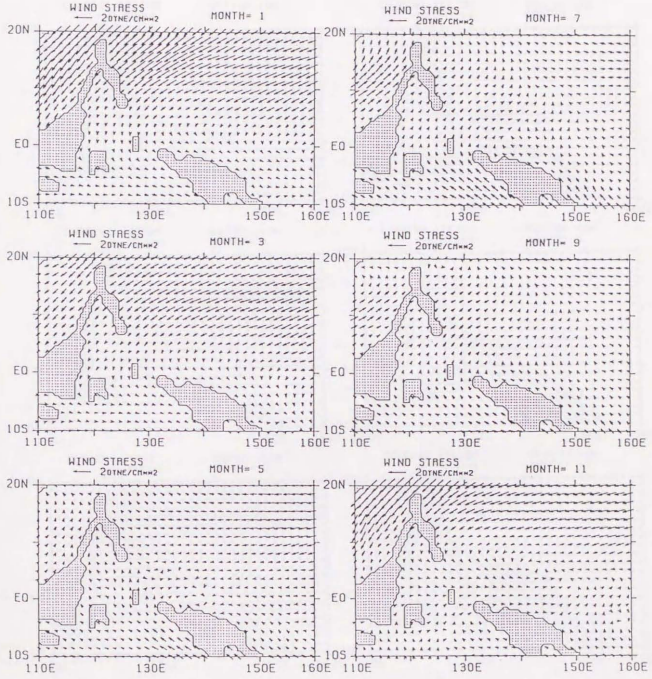

Fig.5. Annual march of revised Hellerman-Rosenstein monthly mean wind stresses.

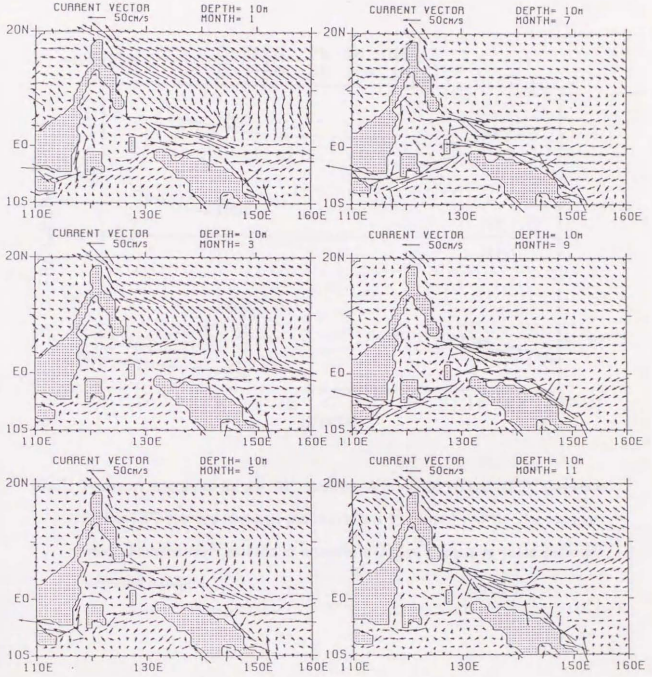

Fig.6. Annual march of horizontal velocity vectors at a depth of 10m.

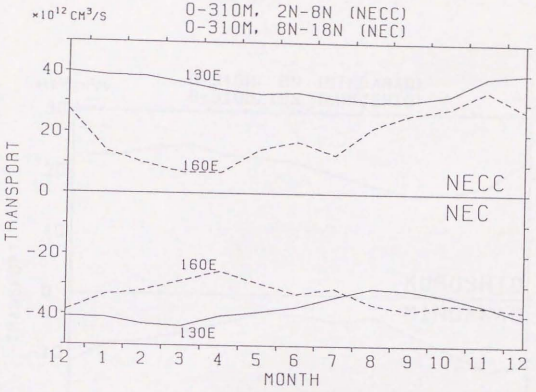

Fig.7. Transport time series for the NEC (between 8°N and 18°N) and NECC (between 2°N and 8°N) across two separated meridians 130°E and 160°E. The transport was calculated from surface to a depth of 310m. Negative value indicates westward transport.

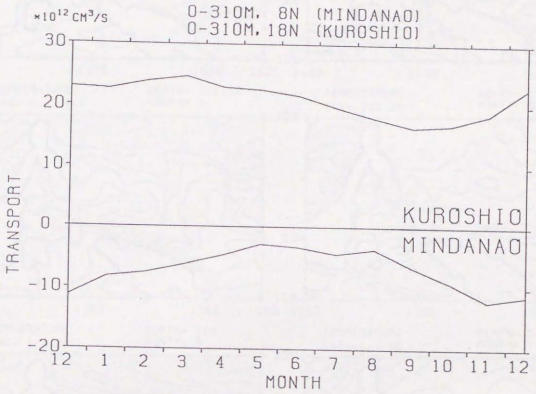

Fig.8. Same as in Fig. 7 but for the Kuroshio across 18°N and the Mindanao Current across 8°N. The transport was calculated from surface to a depth of 310m and between the Philippine coast and 130°E. Negative value indicates southward transport.

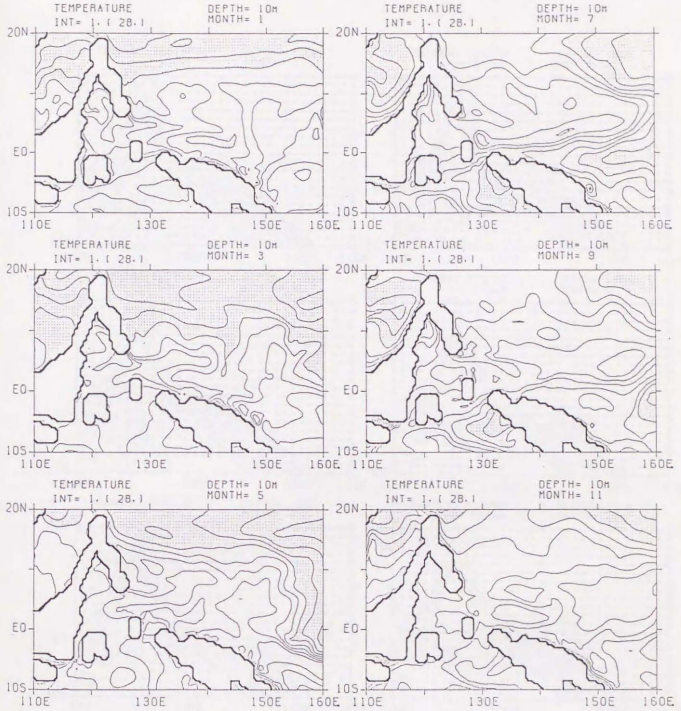

Fig.9. Annual march of surface temperatures at a depth of 10m. Contour interval is 1°C. Temperatures less than 28°C are shaded.

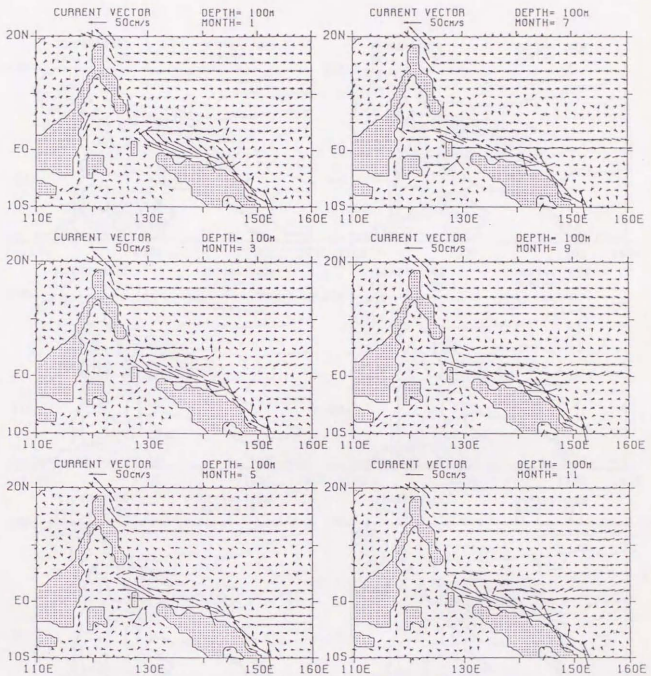

Fig.10. Same as in Fig.6 but for a depth of 100m.

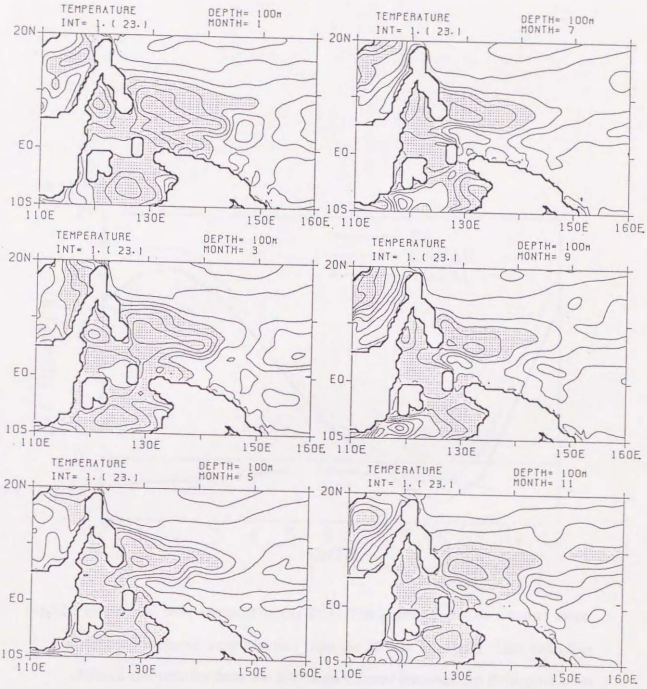

Fig.11. Same as in Fig.9 but for a depth of 100m. Temperatures less than 23°C are shaded.

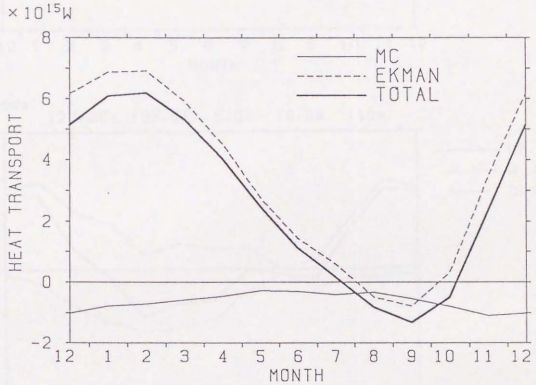

Fig.12. Meridional heat transport across 8°N. Thick solid line shows a total value. Dashed line shows a contribution from the Ekman transport. Thin solid line shows a contribution from the Mindanao Current (between the Philippine coast and 130°E). All transport calculation was done from surface to a depth of 310m.

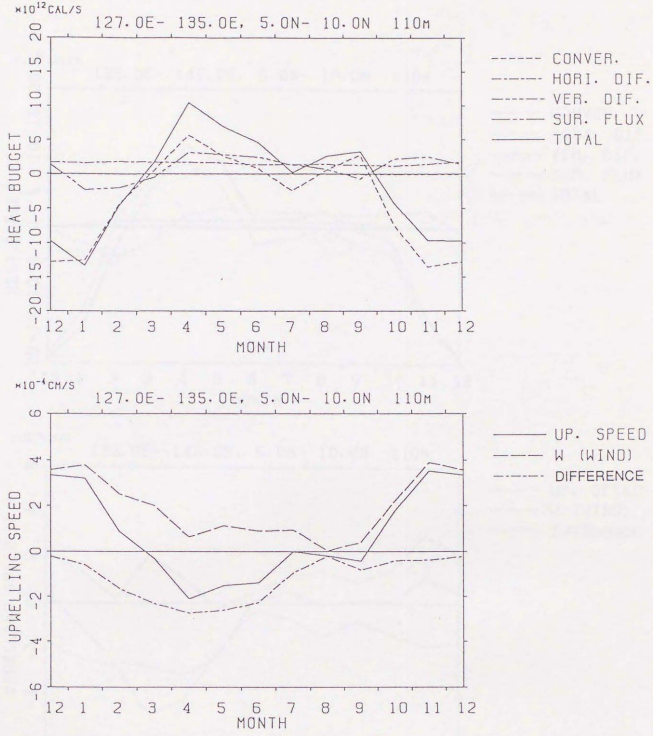

Fig.13. (a): Monthly mean heat budget analysis for the Box A. The rate of change of heat storage is determined by the convergence of heat transport, flux across the surface, horizontal and vertical diffusion. (b): The modelled mean upwelling speed (in 10^{-4} cm/sec) at a depth of 110m for the Box A. The contribution from the Ekman pumping (due to local wind forcing) and the difference between the two (due to remote forcing) are also shown.

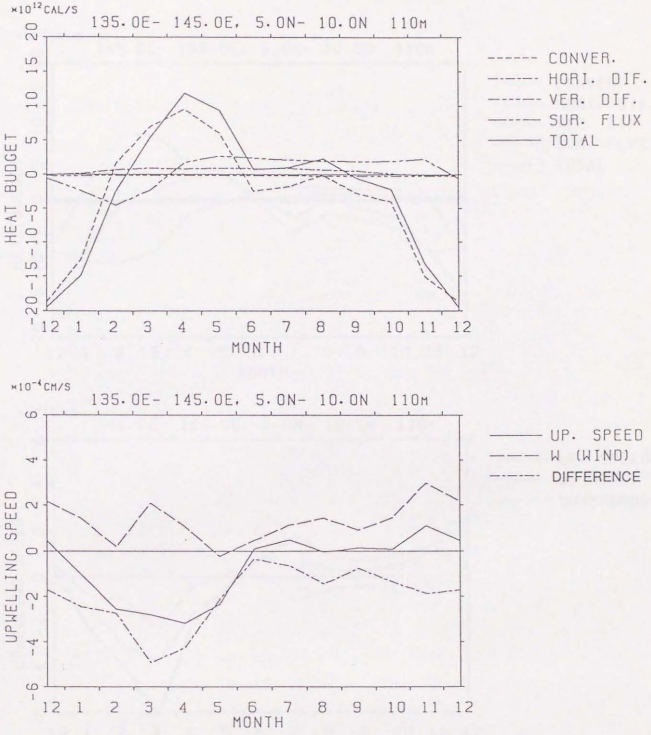

Fig.13. (Continued). Same as in Fig.13(a) and (b) but for the Box B.

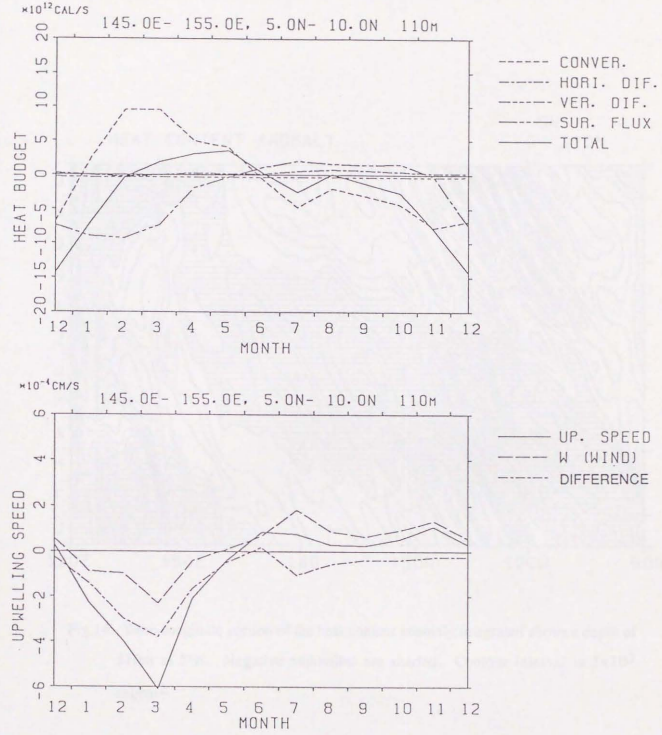

Fig.13. (Continued). Same as in Fig.13(a) and (b) but for the Box C.

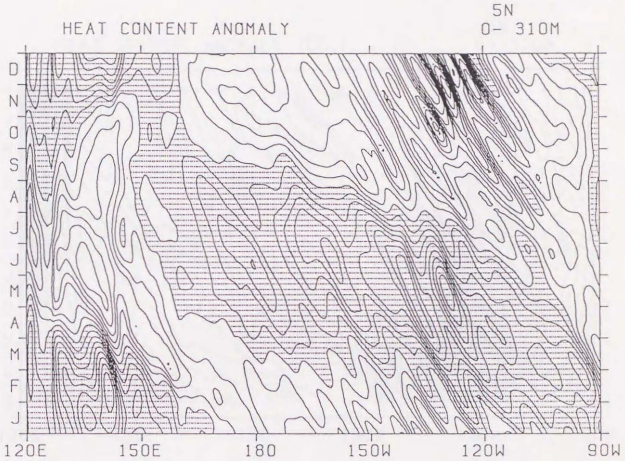

Fig.14. Time-longitude section of the heat content anomaly integrated above a depth of 310m at 5°N. Negative anomalies are shaded. Contour interval is 5×10^3 cal/cm^2.

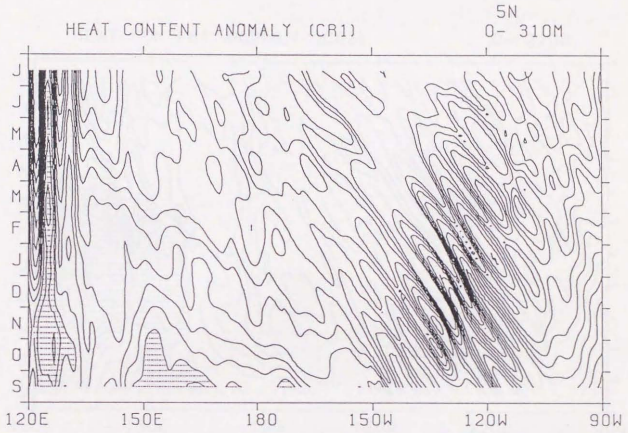

Fig.15. Same as in Fig.14 but for CR 1.

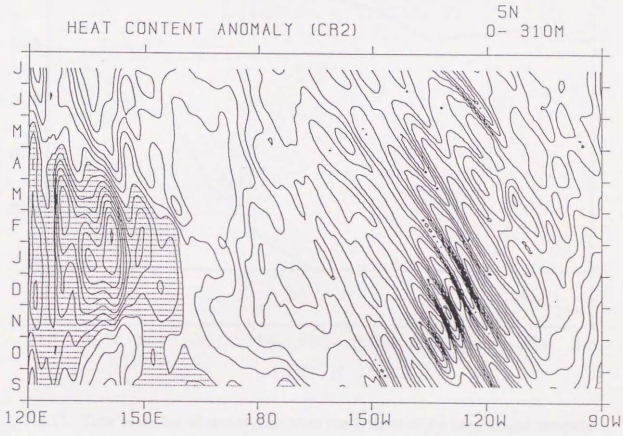

Fig.16. Same as in Fig.14 but for CR 2.

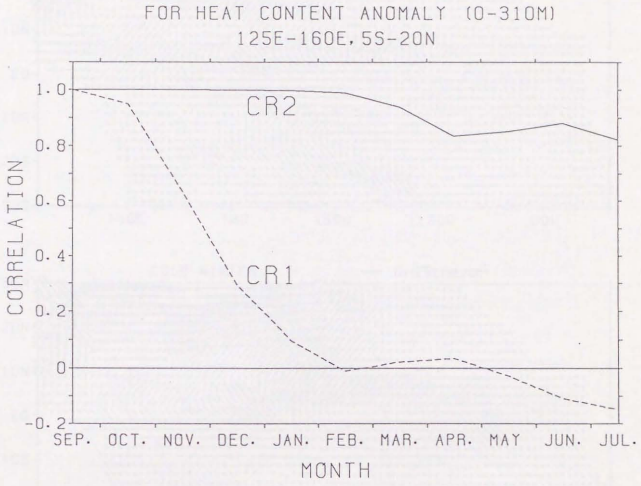

Fig.17. Time evolution of spatial correlation coefficients of the heat content anomaly between the standard run and each of the control runs. The correlation was calculated for the oceanic area from 5°S through 20°N and from 125°E through 160°E.

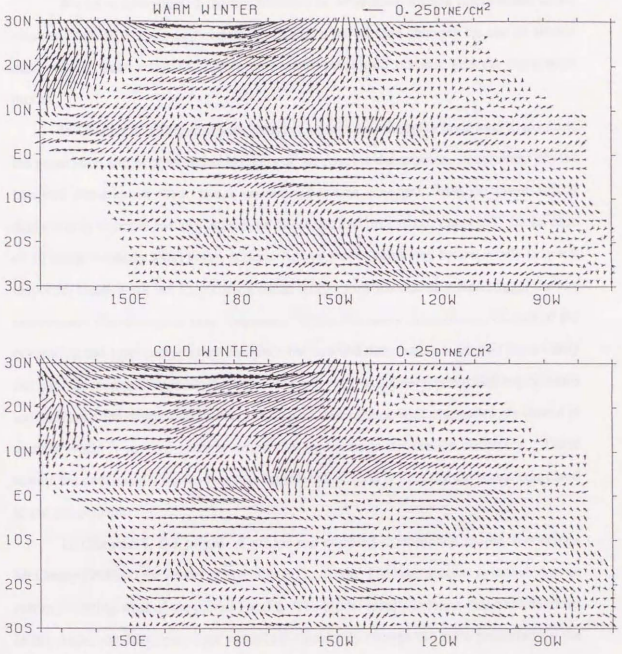

Fig.18. Composite FSU wind stress anomalies classified into warm and cold winters. The anomalies are average of December, January and February. The warm winter consists of 1966, 69, 72, 73, 79 and 83 (the years including January), while the cold winter is composed of 1962, 63, 68, 74 and 84. (Adapted from Hanawa et al. 1989.)

Chapter 5 : Conclusions

We have investigated the mechanisms of large-scale air-sea interactions in the western tropical Pacific associated with short-term climate changes by use of simple atmosphere-ocean coupled models and a fine-resolution oceanic general circulation model.

In Chapter 2, a simple air-sea coupled aqua-planet model is presented to examine the generation and evolution mechanisms of the coupled disturbance. A coherent air-sea coupled disturbance with zonal wavenumber one emerges from different initial disturbances either in the atmosphere or the ocean and propagates eastward. In the case of an initial westerly wind burst, oceanic Kelvin waves generated by the winds (a quick response) cause weak but long-lasting ocean temperature anomalies which trigger the air-sea coupled disturbance (a slow response). When the initial disturbance consists of the oceanic mixed-layer temperature anomaly, the coupled disturbance is excited more easily since the atmosphere responds directly to the anomaly. Additional controlled experiments indicated that the coupled disturbance collapses when the oceanic anomalies are forced to vanish, while it revives quickly when the atmospheric anomalies disappear. These results are consistent with the fact that the relaxation time is long for the ocean compared to the atmosphere.

In Chapter 3, the origin of an air-sea coupled disturbance in the Anderson-McCreary (1985a) type model is investigated in detail. The land process is included as an external heating west of the model Pacific. The model results indicate that nonlinearities in the Anderson-McCreary type models dramatically change the state predicted by the linear theory. The recurrence of the coupled disturbance in the model western Pacific has nothing to do with the linear U1 mode of Hirst (1988) as well as off-equatorial Rossby waves. It is determined by the amplitude of the external heating. The mass budget analysis demonstrates that the change of zonal wind direction in the western Pacific, which is due to the relative importance between the external land heating and the heating associated with the previous coupled disturbance, modulates the oceanic heat content

relevant to the origin of the following coupled disturbance. This mechanism gives an oscillation between two stable equilibria (La Niña and El Niño), which is very different from those described in Battisti (1988), Schopf and Suarez (1988) and Zebiak and Cane (1987).

In Chapter 4, the fine-resolution oceanic general circulation model based on the GFDL model is used to investigate the seasonal variations of the oceanic conditions in the western tropical Pacific, especially the Mindanao Dome. It is found that the model's Mindanao Dome, which evolves in late fall off the Philippine coast due to local upwelling, results from a positive wind-stress curl associated with the northeast Asian winter monsoon. It expands eastward with a recirculation composed of the North Equatorial Current in the north, the Mindanao Current in the west, and the North Equatorial Countercurrent in the south. After reaching a maximum in winter, it begins to decay in spring due to an intrusion of downwelling long Rossby waves excited in winter by the northeast trade winds farther eastward near 160°E, as well as a retreat of the local positive wind-stress curl. Further control runs demonstrate that the variation of the model's Mindanao Dome is almost perfectly determined by the change of the wind field in the western Pacific west of the date line.

The above numerical studies suggest that the Asian monsoon systems, i.e. the coupled ocean-atmosphere-land system, may strongly regulate the seasonal variabilities in the western tropical Pacific. Despite lots of model limitations, the present results seem to be compatible with recent analyses of the air-sea-land system in the western Pacific (cf. Meehl, 1987 ; Yasunari, 1991). Interannual modulation of the seasonal cycle in the coupled system may lead to the atmospheric and/or oceanic anomalies that excite atmosphere-ocean coupled disturbances such as the one associated with the El Niño event. However, in order to clarify the mechanisms that cause the interannual modulation, further investigations using numerical models of various complexity and, in particular, by intensive observations such as the TOGA-TAO array are needed.

Moreover, we saw that the different atmosphere-ocean coupled models of intermediate complexity provided different reasons for giving rise to the oscillatory state. This is also the case for the coupled general circulation models and even for stand-alone ocean or atmosphere models. A careful comparison of those model results with observed data is essential to understand the true mechanism at work in the real world. Thus, in the near future, a synthetic study that includes a theoretical approach, numerical modeling, and an analysis of observed data will be requisite.

REFERENCES

Anderson, D.L.T. and J.P. McCreary, 1985a : Slowly propagating disturbances in a coupled ocean-atmosphere model. *J.Atmos.Sci.*, **42**, 615-629.

Anderson, D.L.T. and J.P. McCreary, 1985b : On the role of the Indian Ocean in a coupled ocean-atmosphere model of El Niño and the the Southern Oscillation. *J.Atmos.Sci.*, **42**, 2439-2442.

Barnett, T.P., 1991 : The interaction of multiple time scales in the tropical climate system. *J.Climate*, **4**, 269-285.

Barnett, T.P., L. Dumenil, U. Schlase, E. Roeckner and M. Latif, 1989 : The effects of Eurasian snow cover on regional and global climate variations. *J.Atmos.Sci.*, **46**, 661-685.

Battisti, D.S., 1988 : The dynamics and thermodynamics of a warming event in a coupled tropical atmosphere/ocean model. *J.Atmos.Sci.*, **45**, 2889-2919.

Battisti, D.S. and A.C. Hirst, 1989 : Interannual variability in a tropical atmosphere-ocean model: influence of the basic state, ocean geometry and nonlinearity. *J.Atmos.Sci.*, **46**, 1687-1712.

Bjerknes, J., 1966 : A possible response of the atmospheric Hadley circulation to equatorial anomalies of ocean temperature. *Tellus*, **18**, 820-829.

Bryan, K., 1969 : A numerical method for the study of the circulation of the world ocean. *J.Computat.Phys.*, **4**, 347-376.

Bryan, K. and M.D. Cox, 1972 : An approximate equation of state for numerical models of ocean circulation. *J.Phys.Oceanogr.*, **2**, 510-514.

Budin, G.R. and M.K. Davey, 1989 : Land effects in a simple model of the tropical coupled ocean-atmosphere. *Tropical ocean-atmosphere newsletter*, **50**, 1-3, (unpublished manuscript).

Busalacchi, A.J., K. Takeuchi and J.J. O'Brien, 1983 : Interannual variability of the equatorial Pacific - revisited. *J.Geophys.Res.*, **88**, 7551-7562.

Cane, M. A., 1986 : El Niño. *Ann. Rev. Earth Planet. Sci.*, **14**, 43-70.

Cox, M.D., 1984 : A primitive equation, 3-dimensional model of the ocean. *GFDL Ocean Group Technical Report,* **1**.

Davey, M.K. and A.E. Gill, 1987 : Experiments on the tropical circulation with a simple moist model. *Quart.J.R.Meteorol.Soc.*, **113**, 1237-1269.

Davey, M.K. and G. Budin, 1989 : Modeling intraseasonal and interannual variability in the tropics. *Phil. Trans. R. Soc. Lond.* **A 329**, 155-166.

Gill, A.E., 1980 : Some simple solutions for heat-induced tropical circulation. *Quart.J.R.Met.Soc.*, **106**, 447-462.

Gill, A.E., 1982 : Studies of moisture effects in simple atmospheric models: the stable case. *Geophys.Astrophys.Fluid Dynamics*, **19**, 119-152.

Gill, A.E., 1983 : An estimation of sea-level and surface-current anomalies during the 1972 El Niño and consequent thermal effects. *J. Phys. Oceanogr.*, **13**, 586-606.

Gill, A.E., 1985 : Elements of coupled ocean-atmosphere models for the tropics, *In: Coupled ocean-atmosphere models*, J.C.J.Nihoul(Ed.), Elsevier,Amsterdam, pp303-327.

Goldenberg, S.B. and J.J. O'Brien, 1981 : Time and space variability of tropical Pacific wind stress. *Mon.Wea.Rev.,* **109**, 1190-1207.

Gordon, C., 1989 : Tropical ocean-atmosphere interactions in a coupled model *Phil.Trans. Roy.Soc. London.* **A 329**, 207-223.

Graham, N.E. and W.B. White, 1988 : The El Niõ cycle: A natural oscillator of the Pacific ocean-atmosphere *Science,* **240**, 1293-1302.

Hacker, P., E. Firing, R. Lukas, P.L. Richardson and C.A. Collins, 1989 : Observations of the low-latitude western boundary circulation in the Pacific during WEPOCS III. *Proceedings of the Western Pacific International Meeting and Workshop on TOGA COARE* (ed. J.Picaut, R.Lukas and T.Delcroix), 135-143.

Hanawa, K, Y. Yoshikawa and T. Watanabe, 1989 : Composite analyses of wintertime wind stress vector fields with respect to SST anomalies in the western north Pacific and the ENSO events Part I:SST composite, *J.Meteor.Soc.Japan*, **67**, 385-400.

Hellerman, S. and M. Rosenstein, 1983 : Normal monthly wind stress over the world ocean with error estimates. *J.Phys.Oceanogr.*, **13**, 1093-1104.

Hirst, A.C., 1986 : Unstable and damped equatorial models in simple coupled ocean-atmosphere models. *J. Atmos. Sci.*, **43**, 606-630.

Hirst, A.C., 1988 : Slow instabilities in tropical ocean basin - global atmosphere models. *J.Atmos.Sci.*, **45**, 830-852.

Hirst, A.C. and K.-M. Lau, 1989 : Intraseasonal and interannual oscillations in coupled ocean-atmosphere models. *J.Climate*, **3**, 713-725.

Keen, R.A., 1982 : The role of cross-equatorial tropical cyclonepairs in the Southern Oscillation. *Mon.Wea.Rev.*, **110**, 1405-1416.

Kendall, T.R., 1989 : Fluctuation of transports and sea level in the western boundary region of the tropical Pacific ocean. *J.Oceanogr.Soc.Japan*, **45**, 279-287.

Kitamura, Y., 1990 : Simulation of the annual and interannual variation of the tropical Pacific ocean. *J.Marine Systems* , **1**, 169-181.

Kubota, M. and J.J. O'Brien, 1988 : Variability of the upper tropical Pacific Ocean model. *J.Geophys.Res.*, **93**, 13930-13940.

Lau, K.-M., 1981 : Oscillations in a simple equatorial climate system *J.Atmos.Sci.*, **38**, 248-261.

Levitus, S., 1982 : Climatological atlas of the world ocean. *NOAA Prof.Paper* **13**, 173pp.,17microfiche, U.S.Govt.Printing Office, Washington D.C.

Lindstrom, E., R. Lukas, R. Fine, E. Firing, S. Godfrey, G. Meyers and M. Tsuchiya, 1987 : The Western Equatorial Pacific Ocean Circulation Study. *Nature*, **330**, 533-537.

Lukas, R., 1988 : Interannual fluctuations of the Mindanao Current inferred from sea level. *J.Geophys.Res.*, **93**, 6744-6748.

Madden, R.A. and P.R. Julian, 1972 : Description of global-scale circulation cells in the tropics with a 40-50 day period. *J.Atmos.Sci.*, **29**, 1109-1123.

Masuzawa, J., 1968 : Second cruise for CSK, Ryofu Maru, January to March 1968. *Oceanogr.Mag.*, **20**, 173-185.

Matsuno, T., 1966 : Quasi-geostrophic motion in the equatorial area. *J.Met.Soc.Japan*, **44**, 25-43.

McCreary, J.P., 1981 : A linear stratified ocean model of the equatorial undercurrent. *Phil.Trans.Roy.Soc.London*, **298**, 603-635.

McCreary, J.P., 1986 : Coupled ocean-atmosphere models of El Niño and the Southern Oscillation. *In: Large-Scale Transport Processes in Oceans and Atmosphere*, (eds. J.Willebrand and D.L.T.Anderson), pp247-280, D.Reidel Publishing Company.

McCreary, J.P. and D.L.T. Anderson, 1991 : An overview of coupled ocean-atmosphere models of El Niño and the Southern Oscillation. *J.Geophys.Res.*, **96**, 3125-3150.

Meehl, G.A., 1987 : The annual cycle and interannual variability in the tropical Pacific and Indian ocean regions. *Mon.Wea.Rev.*, **115**, 27-50.

Mitchum, G.T. and R. Lukas, 1990 : Westward propagation of annual sea level and wind signals in the western Pacific Ocean. *J.Climate*, **3**, 1102-1110.

Nagai, T., T. Tokioka, M. Endoh and Y. Kitamura, 1992 : El Niño-Southern Oscillation simulated in an MRI atmosphere-ocean coupled general circulation model *J.Climate*, **5**, 1202-1233.

Neelin, J.D., M. Latif, M.A.F. Allaart, M.A. Cane, U. Cubasch, W.L. Gates, P.R. Gent, M. Ghil, C. Gordon, N.C. Lau, C.R. Mechoso, G.A. Meehl, J.M. Oberhuber, S.G.H. Philander, P.S. Schopf, K. R. Sperber, A. Sterl, T. Tokioka, J. Tribbia and S.E. Zebiak, 1991 : Tropical air-sea interaction in general circulation models, *Climate Dynamics*, **7**, 73-104.

Nitani, H., 1972 : Beginning of the Kuroshio. In *Kuroshio:Physical aspects of the Japan current*. (ed. H.Stommel and K.Yoshida), pp129-163, University of Washington Press, Seattle.

Nitta, T., 1986 : Long-term variations of cloud amount in the western Pacific region. *J.Met.Soc.Japan*, **64**, 373-390.

Nitta, T., 1989 : Development of a twin cyclone and westerly bursts during the initial phase of the 1986-87 El Niño. *J.Met.Soc.Japan*, **67**, 677-681.

Nitta, T. and T. Motoki, 1987 : Abrupt enhancement of convective activity and low-level westerly burst during the onset of the 1986-87 El Niño. *J.Met.Soc.Japan*, **65**, 497-506.

Pacanowski, R. and S.G.H. Philander, 1981 : Parameterization of vertical mixing in numerical models of tropical oceans. *J.Phys.Oceanogr.*, **11**, 1443-1451.

Philander, S.G.H., T. Yamagata and R.C. Pacanowski, 1984 : Unstable air-sea interactions in the tropics. *J.Atmos.Sci.*, **41**, 604-613.

Philander, S.G.H. and A.D. Seigel, 1985 : Simulation of El Niño of 1982-1983. *Coupled Ocean-Atmosphere Models*. (ed. J.Nihoul), Elsevier, 517-541.

Philander, S.G.H., W.J. Hurlin and R.C. Pacanowski, 1987a : Initial conditions for a general circulation model of tropical oceans. *J.Phys.Oceanogr.*, **17**, 147-157.

Philander, S.G.H., W.J. Hurlin and A.D. Seigel, 1987b : Simulation of the seasonal cycle of the tropical Pacific ocean. *J.Phys.Oceanogr.*, **17**, 1986-2002.

Philander, S.G.H., N.C. Lau, R.C. Pacanowski and M.J. Nath, 1989 : Two different simulations of the Southern Oscillation and El Niño with coupled ocean-atmosphere general circulation models. *Phil.Trans. Roy.Soc. London.* A **329**, 167-178.

Rennick, M.A., 1983 : A model of atmospheric-ocean coupling in El Niō. *Tropical ocean-atmosphere newsletter*, **15**, 2-4, (unpublished manuscript).

Schopf, P.S. and M.J. Suarez, 1988 : Vacillations in a coupled ocean-atmosphere model. *J.Atmos.Sci.*, **45**, 549-566.

Schopf, P.S. and M.J. Suarez, 1990 : Ocean wave dynamics and the time scale of ENSO. *J.Phys.Oceanogr.*, **20**, 629-645.

Schott, V.G., 1939 : Die äquatorialen Strömungen des westlichen Stillen Ozeans. *Ann.Hydrogr.Mar.Meteorol.*, **67**, 247-257.

Takeuchi, K, 1989 : On warm Rossby waves and their relations to ENSO events. *Proceedings of the Western Pacific International Meeting and Workshop on TOGA COARE* (ed. J.Picaut, R.Lukas and T.Delcroix), 329-334.

Toole, J.M., R.C. Millard, Z. Wang and S. Pu, 1990 : Observations of the Pacific North Equatorial Current bifurcation at the Philippine coast. *J.Phys.Oceanogr.*, **20**, 307-318.

Tsuchiya, M., R. Lukas, R.A. Fine, E. Firing and E. Lindstrom, 1989 : Source waters of the Pacific Equatorial Undercurrent. *Prog.Oceanog.*, **23**, 101-147.

Vallis, G.K., 1988 : Conceptual models of El Niño and the Southern Oscillation *J.Geophys.Res.*, **93**, 13979-13991.

Wakata, Y. and E.S. Sarachik, 1990 : Unstable coupled atmosphere-ocean basin modes in the presence of a spatially varying basic state. *J.Atmos.Sci.*, **48**, 2060-2077.

Wang, X-L.and T. Murakami, 1988 : Intraseasonal disturbance activity before, during and after the 1982-83 ENSO. *J.Atmos.Sci.*, **45**, 3754-3770.

White, W.B., G.A. Meyers, J.R. Donguy and S.E. Pazan, 1985 : Short-term climate variability in the thermal structure of the Pacific Ocean during 1979-82. *J.Phys.Oceanogr.*, **15**, 917-935.

White, W.B., S.E. Pazan and M. Inoue, 1987 : Hindcast/forecast of ENSO events based upon the redistribution of observed and model heat content in the western tropical Pacific,1964-86. *J.Phys.Oceanogr.*, **17**, 264-280.

Whitehead, J.A., 1985 : The deflection of a baroclinic jet by a wall in a rotating fluid. *J.Fluid Mech.*, **157**, 79-93.

Wooding, C.M., P.L. Richardson and C.A. Collins, 1990 : Surface drifter measurements in the Western Equatorial Pacific Ocean Circulation Study (WEPOCS III). June 1988-December 1989. *Woods Hole Oceanographic Institution Tech. Rep.*, WHOI-**90-37**, 129pp.

Wyrtki, K., 1961 : Physical oceanography of the southeast Asian waters. *Naga Rep.*, **2**, 195pp.

Wyrtki, K., 1985 : Water displacements in the Pacific and the genesis of El Niño cycles. *J.Geophys.Res.*, **90**, 7129-7132.

Xie, S.-P., A. Kubokawa and K. Hanawa, 1989 : Oscillations with two feedback processes in a coupled ocean-atmosphere model *J.Climate*, **2**, 946-964.

Yamagata, T., 1985 : Stability of a simple air-sea coupled model in the tropics. *In: Coupled ocean-atmosphere models*, J.C.J.Nihoul(Ed.), Elsevier,Amsterdam, 767pp.

Yamagata, T., 1986 : On the recent development of simple, coupled ocean-atmosphere models of ENSO. *J. Oceanogr. Soc. Japan*, **42**, 299-307.

Yamagata, T., 1987 : A simple moist model relevant to the origin of intraseasonal disturbances in the tropics. *J.Met.Soc Japan*, **65**, 153-165.

Yamagata, T. and Y. Masumoto, 1989 : A simple ocean-atmosphere coupled model of the origin of a warm ENSO event. *Phil. Trans. R. Soc. Lond.* **A 329**, 225-236.

Yasunari, T., 1991 : Impact of Indian Monsoon on the coupled atmosphere/ocean system in the tropical Pacific. *Meteorol. Atmos. Phys.*, **44**, 29-42.

Yoshida, K., 1955 : Coastal upwelling off the California coast. *Rec.Oceanogr.Wks.Japan*, **2**, 1-13.

Zebiak, S.E. and M.A. Cane, 1987 : A model El Niño/Southern Oscillation. *Mon.Wea.Rev.*, **115**, 2262-2278.

Appendix

Governing Equations and Boundary Conditions of the OGCM

1. Governing Equations

The oceanic general circulation model used in this study is a continuous stratified three dimensional model, in which the Boussinesq approximation, the hydrostatic approximation, the turbulent mixing hypothesis, and the rigid-lid approximation are utilized. The momentum equations are

$$u_t + \frac{1}{a\cos\phi}[(uu)_\lambda + (v\cos\phi\, u)_\phi] + (wu)_z - fv = -\frac{1}{a\cos\phi}\left(\frac{p}{\rho_0}\right)_\lambda + F^u , \qquad \text{(A1)}$$

$$v_t + \frac{1}{a\cos\phi}[(uv)_\lambda + (v\cos\phi\, v)_\phi] + (wv)_z + fu = -\frac{1}{a}\left(\frac{p}{\rho_0}\right)_\phi + F^v , \qquad \text{(A2)}$$

where (λ, ϕ) denote longitude and latitude, a the radius of the earth, f the Coriolis parameter, p the pressure, ρ_0 the reference density, and u, v, and w are zonal, meridional, and vertical velocity component, respectively. Subscript indicates the derivatives. F^u and F^v represent the turbulent mixing terms and have the form of;

$$F^u = A_V u_{zz} + A_H \frac{1}{a^2}[\nabla^2(u) + (1 - \tan^2\phi)u - 2\frac{\sin\phi}{\cos^2\phi} v_\lambda] , \qquad \text{(A3)}$$

$$F^v = A_V v_{zz} + A_H \frac{1}{a^2}[\nabla^2(v) + (1 - \tan^2\phi)v + 2\frac{\sin\phi}{\cos^2\phi} u_\lambda] , \qquad \text{(A4)}$$

where A_H and A_V are the coefficients of horizontal and vertical viscosity, and $\nabla^2(\mu)$ is defined by

$$\nabla^2(\mu) = \frac{1}{\cos^2\phi}\,\mu_{\lambda\lambda} + \frac{1}{\cos\phi}(\cos\phi\,\mu_\phi)_\phi \,. \tag{A5}$$

The hydrostatic equation is

$$p_z = -\rho g \,, \tag{A6}$$

where g is the acceleration due to gravity, and ρ is the density. The continuity equation is

$$\frac{1}{a\cos\phi}[(u)_\lambda + (v\cos\phi)_\phi] + (w)_z = 0 \,. \tag{A7}$$

The conservation of heat is expressed by the equation as

$$T_t + \frac{1}{a\cos\phi}[(uT)_\lambda + (v\cos\phi\,T)_\phi] + (wT)_z = F^T \,, \tag{A8}$$

where T is the potential temperature, and F^T is the turbulent diffusion term and has the form

$$F^T = (\frac{K_V}{\delta}T_z)_z + K_H\frac{1}{a^2}[\frac{1}{\cos^2\phi}\,T_{\lambda\lambda} + \frac{1}{\cos\phi}(\cos\phi\,T_\phi)_\phi] \,, \tag{A9}$$

where K_H and K_V are the coefficients of horizontal and vertical diffusivity. The density is determined by the equation of the state,

$$\rho = \rho(T, S, z) \,, \tag{A10}$$

where S is salinity, which has a constant value of 35.0 in the present model. In order to calculate the density, we utilized a third-order polynomial equation based on the Knudsen formula (Bryan and Cox, 1972).

The coefficients of the vertical mixing (A_V and K_V) are the function of the vertical stability, and are calculated by following equations.

$$A_V = \frac{A_0}{(1 + \alpha \ R_i)^k} + A_b \, , \tag{A11}$$

$$K_V = \frac{A_V}{1 + \alpha \ R_i} + K_b \, , \tag{A12}$$

where the Richardson number, R_i, is defined by

$$R_i = - \frac{g}{\rho_0} \frac{\rho_z}{u_z^2 + v_z^2} \, , \tag{A13}$$

where A_b and K_b are background mixing parameters. Following Pacanowski and Philander (1981), we adopt the values of 1 cm^2/s for A_b, 0.1 cm^2/s for K_b, 50 cm^2/s for A_0, and k and α have the value of 2 and 5, respectively. The above coefficients are used for the place where the vertical stratification is stable. For the unstable condition, convective adjustment process is adopted, i.e. the vertical diffusivity is assumed to be infinite. Those process is expressed as follows,

$$\delta = \begin{matrix} 1 \ (\rho'_z < 0) \\ 0 \ (\rho'_z > 0). \end{matrix} \tag{A14}$$

where ρ'_z is the local vertical density gradient.

2. Boundary conditions

We apply the no-slip and the adiabatic conditions for the lateral boundaries, i.e.,

$$u, v, T_n = 0 , \tag{A15}$$

where the subscript n denotes a local derivative normal to the boundary.

Upper boundary conditions at the sea surface, z = 0, are

$$\begin{aligned} & w = 0 , \\ & \rho_0 A_V (u_z, v_z) = (\tau^{\lambda}, \tau^{\phi}) , \\ & K_V T_z = \frac{Q}{\rho_0 C_p} , \end{aligned} \tag{A16}$$

where τ^{λ} and τ^{ϕ} are zonal and meridional components of surface wind-stresses, respectively, Q the surface heat flux, and C_p the specific heat of sea water.

Boundary conditions for the bottom , z = -H(λ, ϕ), are

$$\begin{aligned} & w = - \frac{u}{a \cos\phi} H_{\lambda} - \frac{v}{a} H_{\phi} , \\ & \rho_0 A_V (u_z, v_z) = (\tau_B^{\lambda}, \tau_B^{\phi}) , \\ & T_z = 0 , \end{aligned} \tag{A17}$$

where τ_B^{λ}, τ_B^{ϕ} are bottom stress, which are assumed to be zero in the present model.

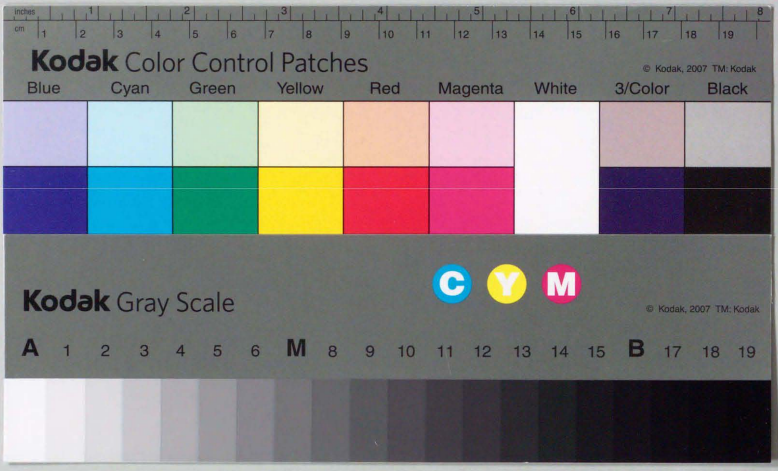
inches
cm
Kodak Color Control Patches
© Kodak, 2007 TM: Kodak
Blue
Cyan
Green
Yellow
Red
Magenta
White
3/Color
Black
Kodak Gray Scale
C
Y
M
© Kodak, 2007 TM: Kodak
A 1 2 3 4 5 6 M 8 9 10 11 12 13 14 15 B 17 18 19